

Mesospheric temperature and circulation response to the Hunga Tonga-Hunga-Ha'apai volcanic eruption

Wandi Yu¹, Rolando R. Garcia², Jia Yue³, Anne K. Smith⁴, Xinyue Wang⁵, William J. Randel⁴, Zishun Qiao⁶, Yunqian Zhu⁷, V. Lynn Harvey⁷, Simone Tilmes⁴, and Martin G. Mlynczak⁸

¹Hampton University

²National Center for Atmospheric Research (NCAR)

³Goddard Space Flight Center

⁴National Center for Atmospheric Research (UCAR)

⁵National Center for Atmospheric Research

⁶Embry-Riddle Aeronautical University

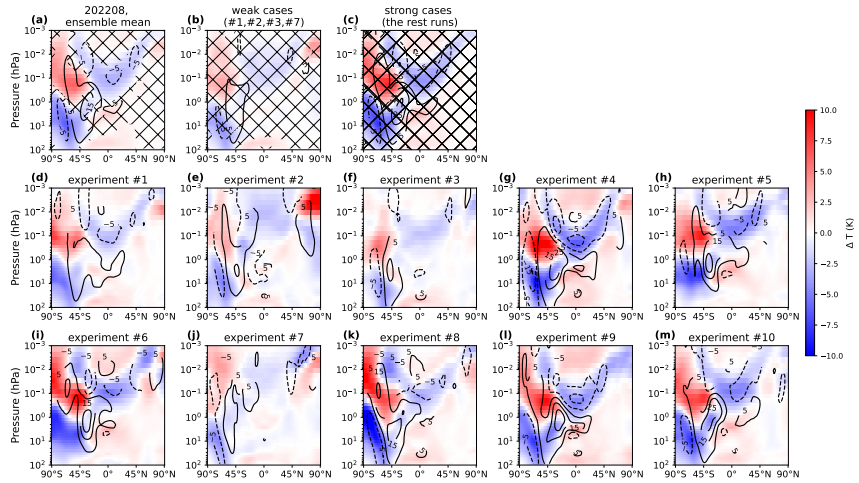
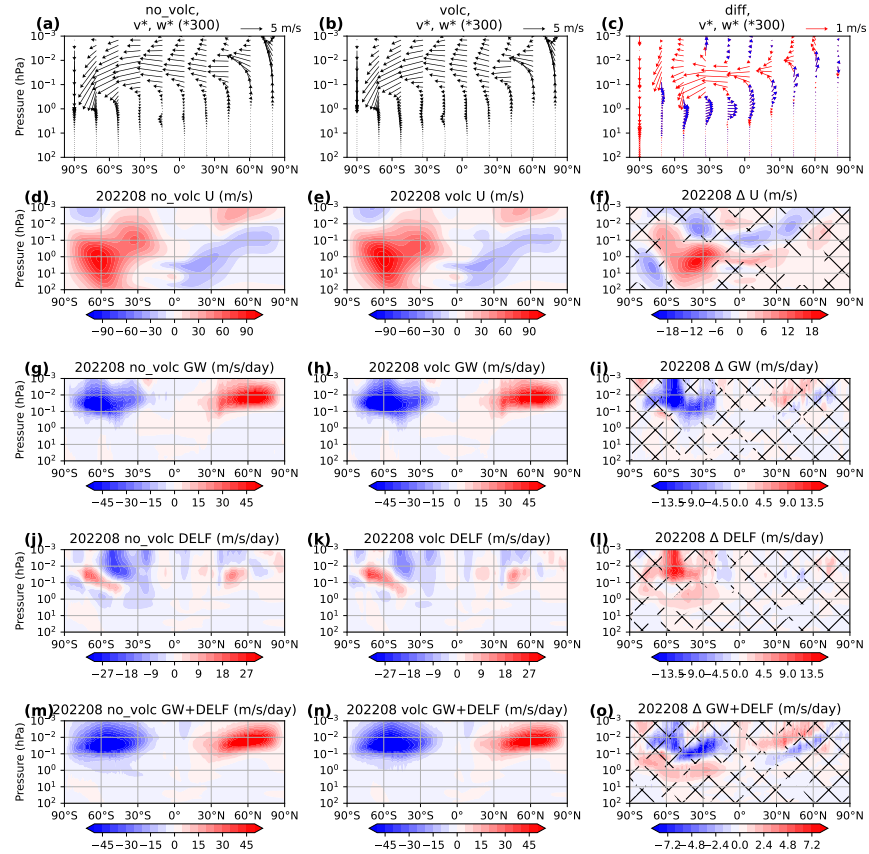
⁷University of Colorado Boulder

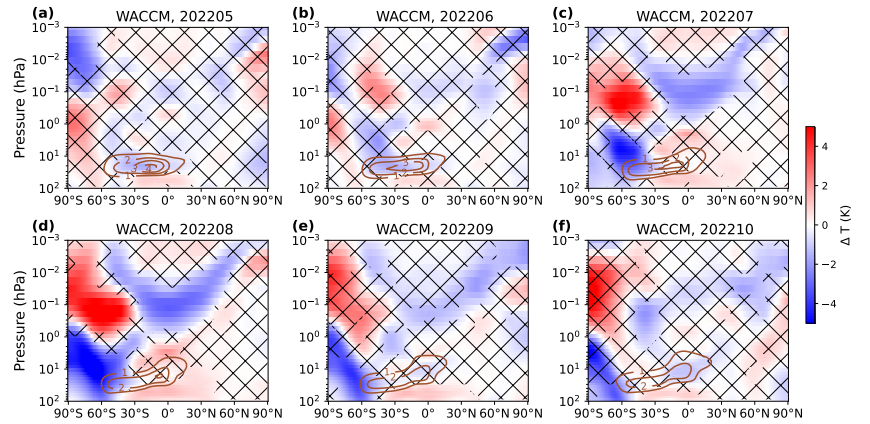
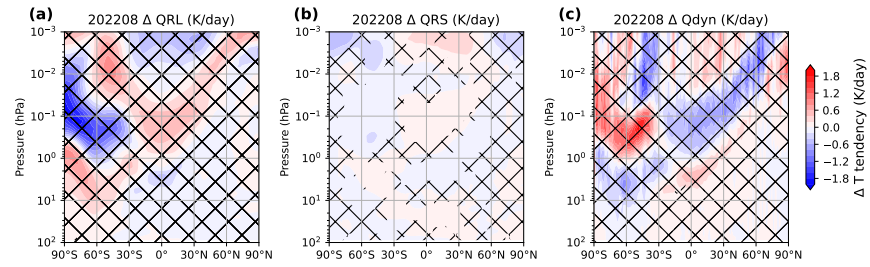
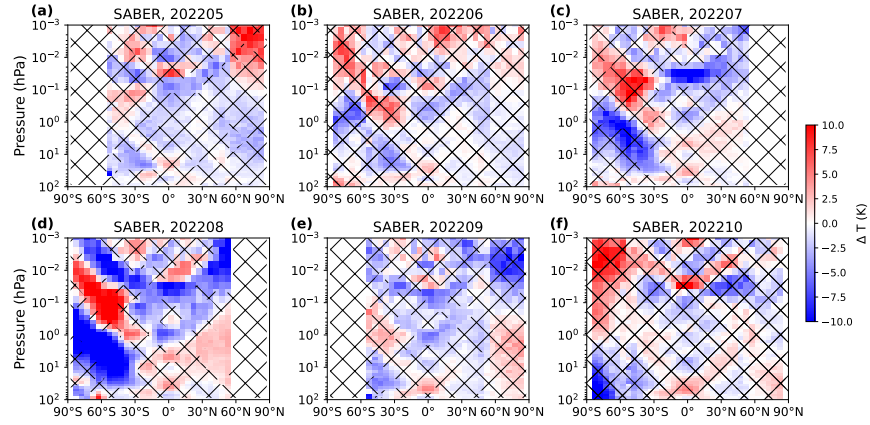
⁸NASA Langley Research Center

July 23, 2023

Abstract

The Hunga Tonga Hunga-Ha'apai (HTHH) volcanic eruption on 15 January 2022 injected water vapor and SO₂ into the stratosphere. Several months after the eruption, significantly stronger westerlies, and a weaker Brewer-Dobson circulation developed in the stratosphere of the Southern Hemisphere and were accompanied by unprecedented temperature anomalies in the stratosphere and mesosphere. In August 2022 the Sounding of the Atmosphere using Broadband Emission Radiometry (SABER) satellite instrument observed record-breaking temperature anomalies in the stratosphere and mesosphere that alternate signs with altitude. Ensemble simulations carried out with the Whole Atmosphere Community Climate Model (WACCM6) indicate that the strengthening of the stratospheric westerlies explains the mesospheric temperature changes. The stronger westerlies cause stronger westward gravity wave drag in the mesosphere, accelerating the mesospheric mean meridional circulation. The stronger mesospheric circulation, in turn, plays a dominant role in driving the changes in mesospheric temperatures. This study highlights the impact of large volcanic eruptions on middle atmospheric dynamics and provides insight into their long-term effects in the mesosphere. On the other hand, we could not discern a clear mechanism for the observed changes in stratospheric circulation. In fact, an examination of the WACCM ensemble reveals that not every member reproduces the large changes observed by SABER. We conclude that there is a stochastic component to the stratospheric response to the HTHH eruption.





Mesospheric temperature and circulation response to the Hunga Tonga-Hunga-Ha'apai volcanic eruption

Wandi Yu¹, Rolando R. Garcia², Jia Yue^{3,4}, Anne K. Smith², Xinyue Wang², William J. Randel², Zishun Qiao⁵, Yunqian Zhu^{6,7}, V.Lynn Harvey^{6,8}, Simone Tilmes², Martin G. Mlynczak⁹

¹Department of Atmospheric and Planetary Sciences, Hampton University, Hampton, VA, USA

²Atmospheric Chemistry Observations & Modeling, National Center for Atmospheric Research, Boulder, CO, USA

³NASA Goddard Space Flight Center, Greenbelt, MD, USA

⁴Catholic University of America, Washington, DC, USA

⁵Embry-Riddle Aeronautical University, FL, USA

⁶Laboratory for Atmospheric and Space Physics, University of Colorado Boulder, Boulder, USA

⁷University of Colorado Cooperative Institute for Research in Environmental Sciences (CIRES) at the

NOAA Chemical Sciences Laboratory, Boulder, CO, USA

⁸Atmospheric and Oceanic Sciences Department, University of Colorado, Boulder, CO, USA

⁹NASA Langley Research Center, Hampton, VA, USA

Key Points:

- SABER observed unprecedented mesospheric temperature variations in the Southern Hemisphere in August 2022 after the HTHH eruption.
- WACCM simulations indicate that changes in the mesospheric temperature are due to a stronger mesospheric meridional circulation.
- Stronger stratospheric westerlies after eruption enhance westward gravity wave drag in the mesosphere, thus a stronger circulation.

Corresponding author: Wandu Yu, wandi.yu@hamptonu.edu

Abstract

The Hunga Tonga Hunga-Ha’apai (HTHH) volcanic eruption on 15 January 2022 injected water vapor and SO_2 into the stratosphere. Several months after the eruption, significantly stronger westerlies, and a weaker Brewer-Dobson circulation developed in the stratosphere of the Southern Hemisphere and were accompanied by unprecedented temperature anomalies in the stratosphere and mesosphere. In August 2022 the Sounding of the Atmosphere using Broadband Emission Radiometry (SABER) satellite instrument observed record-breaking temperature anomalies in the stratosphere and mesosphere that alternate signs with altitude. Ensemble simulations carried out with the Whole Atmosphere Community Climate Model (WACCM6) indicate that the strengthening of the stratospheric westerlies explains the mesospheric temperature changes. The stronger westerlies cause stronger westward gravity wave drag in the mesosphere, accelerating the mesospheric mean meridional circulation. The stronger mesospheric circulation, in turn, plays a dominant role in driving the changes in mesospheric temperatures. This study highlights the impact of large volcanic eruptions on middle atmospheric dynamics and provides insight into their long-term effects in the mesosphere. On the other hand, we could not discern a clear mechanism for the observed changes in stratospheric circulation. In fact, an examination of the WACCM ensemble reveals that not every member reproduces the large changes observed by SABER. We conclude that there is a stochastic component to the stratospheric response to the HTHH eruption.

Plain Language Summary

This work studies the impact of the Hunga Tonga-Hunga Ha’apai volcanic eruption, which took place on January 15, 2022, on the earth’s mesosphere (55 km – 80 km). The eruption injected water vapor and SO_2 into the stratosphere, which was followed by changes in the wind patterns in the stratosphere (16 km – 55 km). Concurrent with these changes, we observed unprecedented temperature changes in the mesosphere, with record high and low temperature anomalies in August that alternate signs with altitude. We used climate model simulations to show that the changes in stratospheric winds were ultimately responsible for these record-breaking mesospheric temperatures. We found that the stronger winds in the stratosphere enhanced gravity wave breaking in the mesosphere, which led to changes in the circulation and thus the temperature. However, we could not find a clear mechanism for the changes observed in the stratosphere.

1 Introduction

On 15 January 2022, a submarine volcano erupted in Hunga Tonga - Hunga Ha’apai (HTHH, 20.54°S, 175.38°W). The volcanic plume reached 55-57 km (Carn et al., 2022; Proud et al., 2022). This eruption injected ~ 50 -150 Tg of water vapor into the stratosphere and increased the total stratospheric water vapor burden by 5-13% reported by different observational instruments (Khaykin et al., 2022; Millán et al., 2022; Randel et al., 2023; Vömel et al., 2022) Meanwhile, 0.4-0.5 Tg of SO_2 was also injected into the stratosphere (Carn et al., 2022), and formed sulfate aerosols (Khaykin et al., 2022; Taha et al., 2022; Zhu et al., 2022).

The HTHH volcanic eruption changed the dynamics in the stratosphere. In the few months following the eruption, the injected water vapor cooled the middle stratosphere and warmed the lower stratosphere; and the sulfate aerosol formed from the injected SO_2 warmed the lower stratosphere (Schoeberl et al., 2022; Sellitto et al., 2022; Wang et al., 2022). These warming and cooling patterns coincide with the distribution of water vapor and sulfate aerosol. However, in the austral winter of 2022, the stratospheric westerly jet shifted equatorward and strengthened, concurrent with a weakening of the stratospheric Brewer-Dobson circulation (Coy et al., 2022; Wang et al., 2022), leading to a depletion of ozone in the mid-latitudes (Wang et al., 2022). At this time, the temperature

74 anomalies consistent with the changes in the stratospheric jet no longer coincided with
75 the location of the water vapor and aerosol anomalies.

76 The mesosphere is the layer of the atmosphere above the stratosphere, from ~ 50
77 km to ~ 85 km, or about 1 hPa to 0.01 hPa. The mesospheric temperature can be en-
78 visaged as being composed of the global mean vertical profile, determined by radiative
79 equilibrium, plus local departures determined mainly by dynamical processes (Andrews
80 et al., 1987). The mesospheric meridional circulation is the most important dynamical
81 process that transports heat and chemical species (Randall et al., 2009; Smith et al., 2011,
82 2010). It is composed of a single, inter-hemispheric cell, with ascent in the summer hemi-
83 sphere and descent in the winter hemisphere, connected by cross-equatorial flow from
84 the summer hemisphere to the winter hemisphere. The circulation is strongest near the
85 two solstices (Dunkerton, 1978). Gravity waves propagating from below, some filtered
86 out by the winds in the stratosphere, break in the mesosphere and deposit angular mo-
87 mentum that drives the mesospheric circulation (Andrews et al., 1987; Garcia & Solomon,
88 1985; Holton, 1983; Lindzen, 1981; Vincent, 2015). The gravity wave breaking that drives
89 the mean meridional circulation is also referred to as “gravity wave drag”.

90 The present study examines the impact of the HTHH volcanic eruption on the mid-
91 dle atmosphere, focusing specifically on changes in temperature and circulation in the
92 mesosphere. By analyzing both satellite observations and model simulations, we aim to
93 address several scientific questions. These include: (1) How does the mesospheric tem-
94 perature respond to the HTHH volcanic eruption? (2) What is the relationship between
95 changes in temperature and the mesospheric circulation that follow the eruption? and
96 (3) What mechanisms contribute to the changes in mesospheric circulation following the
97 eruption? We also discuss our attempts to understand the changes in stratospheric dy-
98 namics following the eruption, whose origin remains unclear.

99 2 Data and Model

100 The Sounding of the Atmosphere using Broadband Emission Radiometry (SABER)
101 instrument onboard NASA’s TIMED (Thermosphere Ionosphere Mesosphere Energet-
102 ics Dynamics) satellite has been measuring temperature and chemical species in the mid-
103 dle atmosphere since January 2002 (Russell et al., 1999). To prevent the SABER detec-
104 tor from pointing directly at the Sun, TIMED performs a “yaw maneuver” that switches
105 coverage from $83^{\circ}\text{S} - 53^{\circ}\text{N}$ to $83^{\circ}\text{N} - 53^{\circ}\text{S}$ every 60 days. SABER temperature data was
106 validated by Dawkins et al. (2018), García-Comas et al. (2008), and Remsberg et al. (2008),
107 and the stability of SABER calibration was examined by Mlynczak et al. (2020). The
108 SABER temperature product covers the altitude range from the tropopause (~ 17 km)
109 to 110 km. In the mesosphere, the SABER temperature product has a vertical resolu-
110 tion of about 2 km, and we grid it into 5° latitude by 10° longitude bins. We use v2.07
111 of the SABER temperature product before December 2019, and v2.08 thereafter (Mlynczak
112 et al., 2023). We use SABER temperature from 2003 to 2022, to avoid the possibility
113 of errors due to the icing on the detector in the first year of operation (Remsberg et al.,
114 2008).

115 We use NCAR’s Whole Atmosphere Community Climate Model (WACCM6; Get-
116 telman et al., 2019) to analyze the dynamic response of the stratosphere and mesosphere
117 to volcanic eruption. This version of WACCM has 70 vertical layers and a horizontal res-
118 olution of 0.95° latitude by 1.25° longitude. We carried out two sets of experiments, each
119 with 10 ensemble members. In the control ensemble, we nudge the temperature and wind
120 field to the GEOS5 meteorological analysis data (Rienecker et al., 2018) throughout Jan-
121 uary 2022 until the beginning of February. The only difference between the ensemble mem-
122 bers is that nudging ends on slightly different dates, in the range from 27 January 2022
123 to 5 February 2022. Once nudging end, the model runs freely and fully coupled to the
124 ocean, sea-ice, and land. The volcanic eruption ensemble applies the same settings as

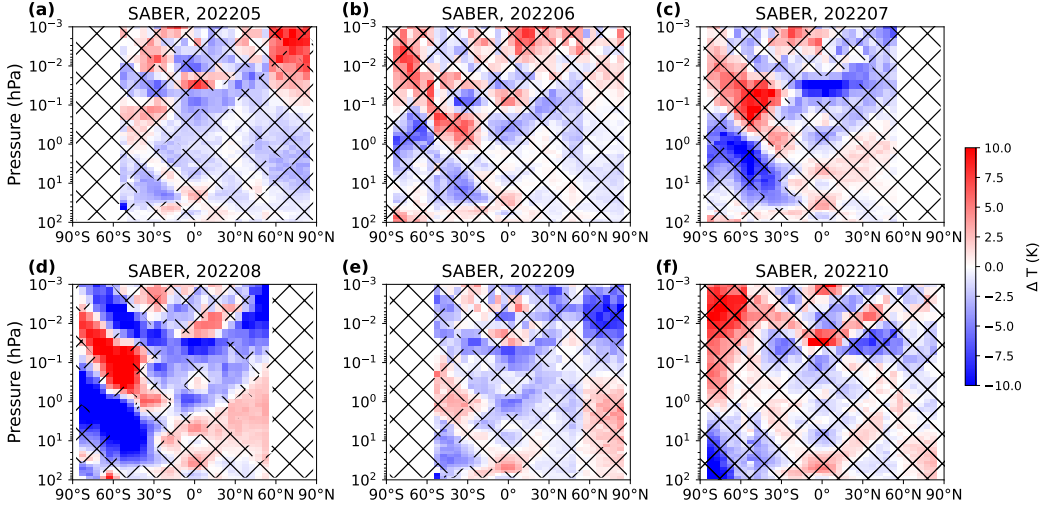


Figure 1. Monthly mean zonal mean temperature anomalies (2022 minus climatology) observed by SABER; the areas without hatching meet two thresholds: (1) must be outside of previous SABER variability and (2) exceed two standard deviations from the climatology. The plots cover the period from May to October 2022.

125 the control group but with the addition of the volcanic forcings. We inject 150 Tg of wa-
 126 ter vapor and 0.42 Tg SO_2 on January 15 following Zhu et al. (2022). Wang et al. (2022)
 127 have already demonstrated that this model setting successfully reproduces satellite ob-
 128 servations of stratospheric dynamics following the HTHH volcanic eruption.

129 3 Results

130 The middle atmospheric temperature observed by SABER in 2022 displayed sig-
 131 nificant anomalies compared to the climatology of the previous 20 years of observations.
 132 Positive and negative anomalies in mesospheric temperature that exceeded both the high
 133 or low values in the historical record and two standard deviations from the climatolog-
 134 ical mean were occasionally observed, as shown in Fig. 1 (areas not covered by hatch-
 135 ing). Some 2022 temperatures can be record-breaking but within 2 sigmas of the clima-
 136 tological mean, while some can exceed the 2-sigma threshold but not be record-breaking.
 137 Thus, we use both criteria jointly as an indication of statistical significance. The peak
 138 temperature anomalies occurred in July and August, revealing a tripolar pattern char-
 139 acterized by a cold center in the Southern Hemisphere (SH) extratropical stratosphere,
 140 a warm center in the mid-latitude mesosphere, and V-shaped cold anomalies extending
 141 from the lower mesosphere in the tropics to the upper mesosphere in the extratropics
 142 in both hemispheres, as shown in Fig. 1c-d. Notably, in August 2022, the mesospheric
 143 temperature in the tripolar structure reached record lows or highs for the entire SABER
 144 era (2003-2022). The August temperature anomalies are as large as ± 10 K in the strato-
 145 sphere and mesosphere. This tripolar structure weakens in September and the signifi-
 146 cant anomalies dissipate after September 2022. We compared SABER temperature anom-
 147 alies with those from the Microwave Limb Sounder (MLS, Livesey et al., 2020; Waters et
 148 al., 2006) v5.0 temperature product (not shown), which has a better vertical resolution
 149 in the stratosphere and has global coverage but a coarser vertical resolution in the meso-
 150 sphere, and draw the same conclusion.

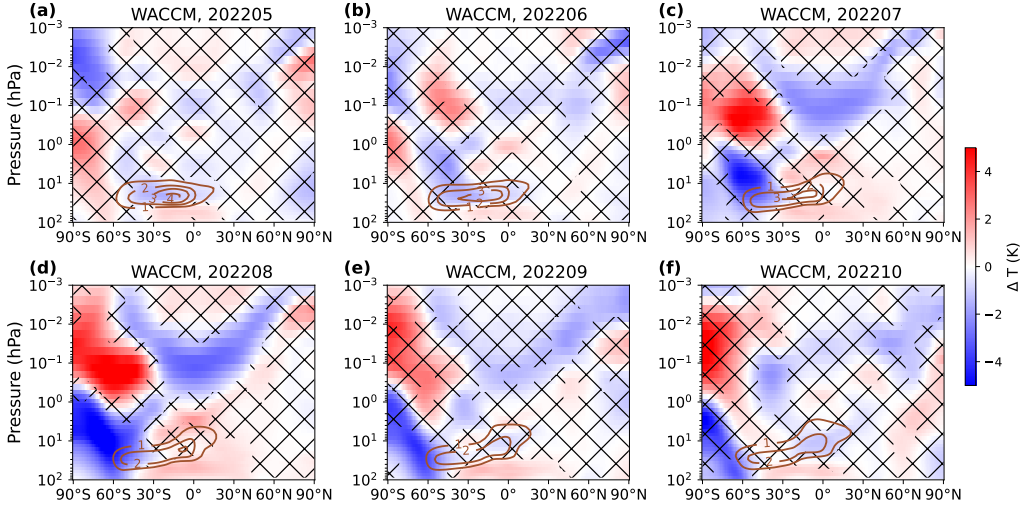


Figure 2. The 10-ensemble mean monthly mean zonal mean temperature difference between the volcano run and the control run in WACCM. The areas with differences that have a p-value > 0.05 in a Student’s t-test are indicated by hatching. The plots cover the period from May to October 2022. Brown contours show zonal mean water vapor mixing ratio anomalies in ppmv.

151 To untangle the influence of the volcanic eruption from internal variability on changes
 152 in mesospheric temperature, we performed WACCM simulations where the only differ-
 153 ence with respect to the control ensemble is whether H_2O and SO_2 are injected. We ran
 154 fully coupled free-running WACCM after February 2022 to capture the interaction be-
 155 tween composition and circulation. In Fig. 2, we show the temperature difference (ΔT)
 156 between the ensemble means of the WACCM volcano case and the control case. The en-
 157 semble mean ΔT (the difference between the volcanic and control ensemble means) in-
 158 creased over time, exhibiting the same significant tripolar structure as that observed by
 159 SABER in July and August, with the structure weakening after September. The mod-
 160 eled ensemble mean ΔT pattern mirrors the observed tripolar structure. The magni-
 161 tude of the ensemble-average signal is, however, 40% of that seen in the observations.

162 We examined the members of the volcanic ensemble individually for August 2022,
 163 comparing each one against the mean of the control ensemble. All ten volcanic ensem-
 164 ble members reproduce the observed temperature anomaly pattern in that month; six
 165 out of ten have an anomaly amplitude comparable to the observations (Figs. 3g-i and
 166 3k-m); and four show a smaller amplitude (Figs. 3d-f and 3j). We refer to the six cases
 167 with a signal amplitude that is comparable to observations as “strong” cases, and to the
 168 other four cases as “weak” cases. The strong and weak cases occur independently of the
 169 date when nudging was stopped. The ensemble mean of the strong cases shows a signif-
 170 icant tripolar structure with magnitudes comparable to the observations, with a max-
 171 imum ΔT of ± 10 K in the stratosphere and mesosphere (Fig. 3c). These results may
 172 be summarized as follows: (1) all ten cases can reproduce the observed spatial structure
 173 indicating that the HTHH forcing is very likely the cause of the observed anomaly; and
 174 (2) a substantial fraction (40%) of the volcanic eruption simulations has a weak signal,
 175 indicating that there is a substantial stochastic component, such that the observed re-
 176 sponse is likely but not entirely deterministic.

177 We attempted to find a mechanistic explanation for the stratospheric temperature
 178 anomalies that develop in the months following the eruption but were unable to do so.
 179 At the same time when strong stratospheric temperature anomalies occur, there is a stronger

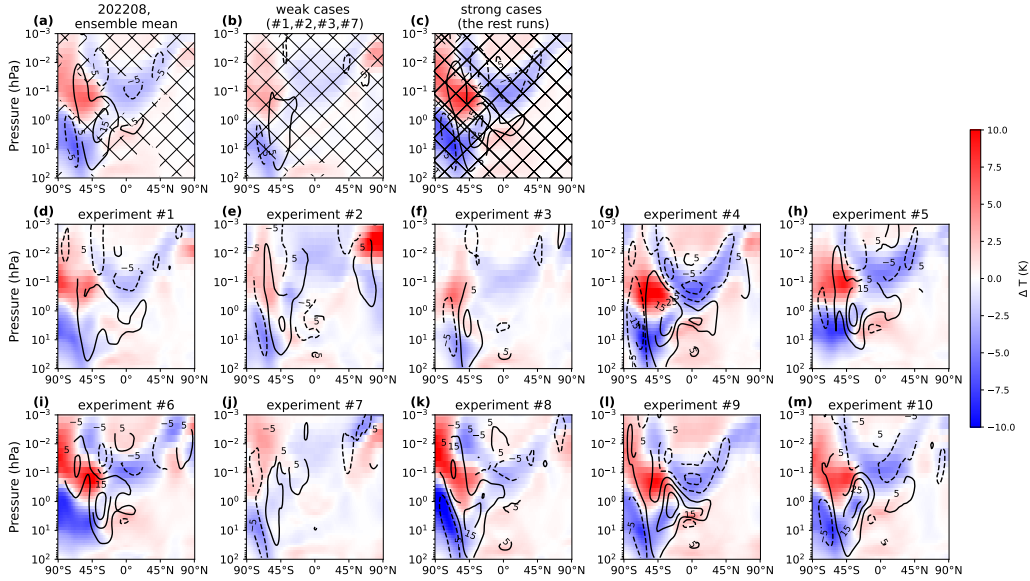


Figure 3. August 2022 zonal mean temperature difference (shading) between the volcano run and the ensemble mean control run in WACCM averaged over (a) all 10 volcanic ensemble members, (b) volcanic weak cases (case numbers 4,5,7), and (c) volcanic strong cases (the remainder of the cases in the volcanic ensemble). The areas with differences that have a p-value > 0.05 in a t-test are indicated by hatching. (d-m) The zonal mean temperature difference and zonal wind difference (contour) between each volcano run and the ensemble mean control run in WACCM. The date when nudging ends in WACCM is 27 January 2022 to 5 February 2022 in cases 1-10, respectively.

180 polar jet, a weakening in the planetary wave amplitude (mostly zonal wave 1), and thus
 181 weakening planetary wave drag (EP flux divergence) over SH mid-latitudes. This is a
 182 pattern of natural internal variability has been described in previous studies (e.g. Holton
 183 & Mass, 1976; Randel & Newman, 1998). We investigated the role of possible precu-
 184 sors to this pattern, in the months immediately following the eruption and before June,
 185 but we did not find statistically significant differences among the August strong and weak
 186 cases. The precursors we examined include radiative forcing from water vapor or sulfate
 187 aerosols, gravity wave drag, planetary wave propagation conditions, EP flux and EP flux
 188 divergence, meridional and zonal wind, and tropical and subtropical temperatures. We
 189 also examined the behavior of the quasi-biennial oscillation and found no statistically
 190 significant differences in amplitude or phase. Furthermore, we found that the strong and
 191 weak cases in July but are not always the same as the strong and weak cases in August.
 192 Finally, we have identified similar patterns of stratospheric temperature anomalies, al-
 193 though with somewhat weaker amplitude (within ± 7 K), to those observed in August
 194 in three control cases where no volcanic forcing is present. We conclude from these WACCM6
 195 simulations that the strong July/August response in stratospheric temperature is partly
 196 stochastic, although the volcanic forcing (H_2O+SO_2) significantly increases the proba-
 197 bility that the system will develop the observed SH system.

198 In contrast to the stratosphere, it is relatively simple to understand mechanistically
 199 the development of mesospheric temperature anomalies once the stratospheric changes
 200 are in place. In what follows, we focus on August 2022, the month with the strongest
 201 temperature response in both the stratosphere and mesosphere. We partition the meso-

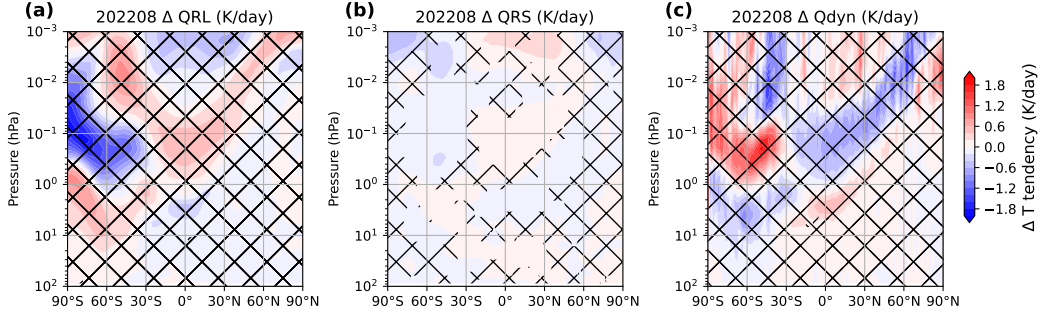


Figure 4. Latitude-pressure distribution of terms in the zonal-mean temperature budget in WACCM in August of 2022. The plots show the 10-member ensemble mean difference between the volcano case and the control case for (a) longwave heating rate, (b) shortwave heating rate, and (c) heating rate related to dynamics. The areas with differences that have a p-value > 0.05 in a t-test are indicated by hatching.

202 spheric temperature budget into contributions from radiation and dynamics, using the
 203 transformed Eulerian mean (TEM) thermodynamic equation (Andrews et al., 1987):

$$\frac{\partial \bar{T}}{\partial t} = -w^* S - v^* \frac{\partial \bar{T}}{a \partial \phi} + QRL + QRS \quad (1)$$

204 Where $\frac{\partial \bar{T}}{\partial t}$ is the rate of temperature change, v^* and w^* are the TEM meridional
 205 and vertical velocities, S is the static stability, QRL and QRS are the longwave and short-
 206 wave heating rates, a is the Earth’s radius and ϕ is latitude. On a monthly mean basis,
 207 $\frac{\partial \bar{T}}{\partial t}$ is expected to be small, and QRL reflects the changes in temperature (Wehrbein &
 208 Leovy, 1982), so we have:

$$QRL = -(Q_{dyn} + QRS) \quad (2)$$

209 where:

$$Q_{dyn} = -w^* S - v^* \frac{\partial \bar{T}}{a \partial \phi} \quad (3)$$

210 Our model results suggest that changes in dynamics (which produce adiabatic cool-
 211 ing or warming) are the primary contributor to mesospheric temperature changes (Fig.
 212 4). Although there are some regions where the difference in the mesospheric shortwave
 213 heating rate between the volcano case and control case is significant, changes in short-
 214 wave heating rate in response to the volcanic eruption are negligible with respect to other
 215 terms in Eq. (1).

216 The mean meridional circulation determines Q_{dyn} in the mesosphere. Following the
 217 HTHH eruption, there was a $\sim 20\%$ strengthening of the mesospheric mean meridional
 218 circulation, which peaked in August of 2022, as shown by the red arrows in Fig. 5c. The
 219 polar winter SH shows strongly enhanced descending motion of $\sim 0.003 \text{ ms}^{-1}$ between
 220 0.1 hPa and 0.01 hPa, corresponding to the warm temperature anomaly seen in Fig. 3.
 221 In the summer Northern Hemisphere (NH), there is a weak acceleration in the ascend-
 222 ing motion of $\sim 0.002 \text{ ms}^{-1}$ above 0.1 hPa. In the tropical regions of both hemispheres,
 223 the horizontal mean flow accelerates by $\sim 1 \text{ ms}^{-1}$ at around 0.1 hPa. The acceleration

224 of the mesospheric circulation in the tropics and the summer hemisphere coincides with
 225 the V-shaped region of cooling there (Fig. 2).

226 We attribute the strengthening of the mean meridional circulation in the mesosphere
 227 to the strengthening of the stratospheric westerlies, and their resultant effects on filter-
 228 ing vertically propagating gravity waves. As mentioned by Coy et al. (2022) and Wang
 229 et al. (2022), the stratospheric westerlies undergo strengthening and an equatorward shift
 230 in SH winter 2022, and this is also what we find in the ensemble of the volcanic simu-
 231 lations (see Fig. 5f). These stratospheric zonal wind changes are in balance with reduced
 232 planetary wave EP flux divergences (Fig. 5l). Changes in the stratospheric westerlies are
 233 consistent with the geostrophic wind that is derived from the meridional temperature
 234 gradient (Harvey et al., 2022; Holton, 2004, p.200) The strengthening of the stratospheric
 235 westerly jet between about 20°S and 60°S filters eastward propagating gravity waves in
 236 the (parameterized) gravity wave spectrum. This, in turn, enhances the net westward
 237 momentum flux reaching the mesosphere. As a result, westward gravity wave drag in-
 238 creases above 0.1 hPa (i.e., the drag becomes more negative, Fig. 5i), which accelerates
 239 the mesospheric meridional circulation in SH mid-latitudes above the region where the
 240 stratospheric westerlies have intensified (Fig. 5c). Although the forcing due to planetary
 241 waves in the mid-latitudes of the SH mesosphere weakens, as shown by the reduced (less
 242 negative) EP-flux divergence in Fig. 5l, it offsets only partially the increase in westward
 243 momentum deposited by the stronger gravity wave breaking. The combination of grav-
 244 ity wave drag and EP flux divergence produces a negative forcing anomaly (Fig. 5o) that
 245 is consistent with the acceleration of the meridional circulation seen in Fig. 5c.

246 The effect of the changes in the mean meridional circulation is reflected in the pat-
 247 tern of Q_{dyn} in the SH mid-latitudes shown in Fig. 4c. The acceleration of the merid-
 248 ional circulation in the SH mid-latitudes extends across the tropics and into the NH, show-
 249 ing a pattern similar to that found during interhemispheric coupling events, along with
 250 concomitant changes in temperature and zonal wind (cf. Smith et al., 2020, their Fig.4).
 251 Changes in gravity wave drag are also reflected in changes in the mesospheric zonal wind
 252 (Fig. 5f) since wave drag tends to accelerate or decelerate the mean flow toward the wave
 253 phase speed. An increase in the westward wave drag between 0.1 – 0.2 hPa in the sub-
 254 tropics leads to a weakening of the eastward zonal wind of $\sim 10 \text{ m s}^{-1}$ there.

255 4 Discussion

256 In 2022, SABER stratospheric and mesospheric temperatures exhibited statistically
 257 significant changes, with record highs and lows observed in the stratosphere and meso-
 258 sphere in August. Our study, based on fully-coupled simulations carried out with WACCM,
 259 shows good agreement with the observed temperature anomalies in the mesosphere. The
 260 model suggests the temperature anomalies in the mesosphere are a result of a global strength-
 261 ening of the mesospheric meridional circulation of $\sim 20\%$. Through our analysis of the
 262 model, we have found that the changes in mesospheric dynamics observed in response
 263 to the HTHH volcanic eruption can be linked to dynamical changes occurring in the strato-
 264 sphere, such as the strengthening of the westerlies, altered gravity wave propagation, the
 265 weakening of planetary wave dissipation, and the weakening of the Brewer-Dobson cir-
 266 culation.

267 The causal relationship between strengthening of the stratospheric westerlies and
 268 the mesospheric temperature anomalies is robust. In all the strong cases of the WACCM
 269 volcanic ensemble where the temperature field tripolar structure has an amplitude com-
 270 parable to the observations, there is a strong strengthening and equatorward shift of the
 271 stratospheric westerlies, and in all the weak cases the stratospheric westerlies strengthen
 272 only weakly (Fig. 3). The timing of the strongest response in the mesosphere in 2022
 273 also indicates that changes in the stratosphere are the cause of the changes in the meso-
 274 sphere. The mesospheric circulation is strongest near the solstice, while in June the tem-

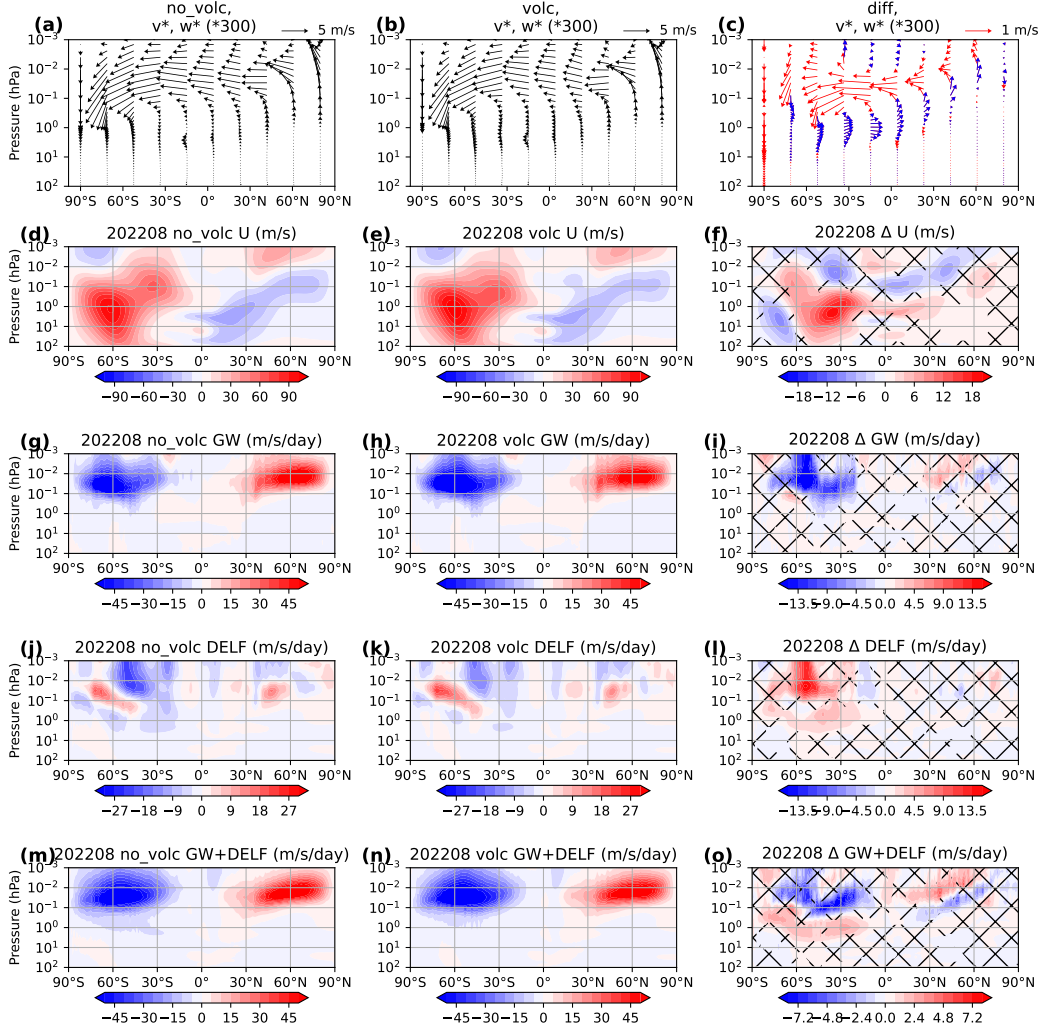


Figure 5. Zonal mean distribution of the WACCM 10-member ensemble mean for various quantities in August of 2022. (a-c) TEM circulation vectors (v^* and $300 \times w^*$ for scaling), (d-f) zonal wind, (g-i) gravity wave drag, (j-l) EP-flux divergence, and (m-o) gravity wave drag plus the EP-flux divergence. The left column shows the control case, the middle column shows the volcano case, and the right column shows the difference between the volcano case minus the control case, where the areas with differences that have a p-value > 0.05 in a t-test are indicated by hatching. In (c), red arrows indicate a strengthening of the mean meridional velocity vector and blue arrows indicate a weakening thereof compared to the control case.

275 perature difference is insignificant. The strongest mesospheric temperature response oc-
 276 curs in August when the strengthening of the westerlies is largest in the stratosphere.
 277 It is also worth mentioning that in early 2023 neither the model nor the observations show
 278 a strong disturbance in stratospheric westerlies, or in the mesospheric temperature and
 279 circulation.

280 Since what happens in the mesosphere is a response to changes in the stratosphere,
 281 there are questions regarding changes in stratospheric dynamics itself. The facts that
 282 (1) not every member of the ensemble reproduces well the observed changes, and (2) the
 283 ensemble members that reproduce most closely the observed changes are not the same
 284 in July and August suggest that there is a stochastic component in the model results.
 285 We also attempted to find precursors for the changes in the stratosphere (radiative forc-
 286 ing, EP fluxes, meridional and zonal winds, tropical and subtropical temperatures), but
 287 were unable to find any statistically significant precursors for the large, significant changes
 288 that take place in July and August in the strong group of volcano ensemble members.

289 There remain many unsolved questions related to the abrupt changes seen in the
 290 stratosphere after the HTHH eruption. For example, what is the initial driver for the
 291 strong reduction of the SH planetary wave drag in the stratosphere in July and August?
 292 Is it the injected water vapor or the aerosols, or something else? Coy et al. (2022) sug-
 293 gested that the changes before June are due to the injected water vapor. As shown in
 294 our Fig. 2, there is a significant cooling in the stratosphere collocated with the injected
 295 water vapor anomaly before June. However, starting in June, a large, negative strato-
 296 spheric temperature anomaly develops in the midlatitudes of the SH over a much broader
 297 altitude range. Since this anomaly is no longer collocated with the water vapor anomaly,
 298 it must be due to dynamical changes. However, as noted above, we were unable to iden-
 299 tify any precursors to these changes. In addition, it is unclear why the stratospheric wind
 300 and circulation anomalies intensify suddenly in July and August. While the investiga-
 301 tion of these stratospheric questions is outside the scope of our paper, addressing them
 302 would enhance our understanding of middle atmospheric dynamics and provide further
 303 insights into the HTHH volcanic eruption.

304 5 Open Research

305 - [Dataset] SABER v2.07 and v2.08 temperature data are available from [https://](https://saber.gats-inc.com/data_services.php)
 306 saber.gats-inc.com/data_services.php, See Mlynczak et al. (2023)

307 - [Software] CESM2-WACCM6 codes are available from [//www.cesm.ucar.edu/](http://www.cesm.ucar.edu/models/cesm2)
 308 [models/cesm2](http://www.cesm.ucar.edu/models/cesm2). See Gettelman et al. (2019).

309 Acknowledgments

310 WY, RG, JY, and MM are supported by the TIMED/SABER mission from the NASA
 311 Heliophysics Division. WY and JY are also supported by NASA’s Heliophysics Division
 312 AIM mission and NSF AGS1901126. RG is supported in part by NASA grant 80NSSC19K1214.
 313 ZQ is supported by NSF AGS-1828589. The National Center for Atmospheric Research
 314 is sponsored by the National Science Foundation. Work conducted at CIRES/NOAA is
 315 supported by the NOAA’s Earth Radiation Budget (ERB) Initiative (CPO #03-01-07-
 316 001), and in part by NOAA cooperative agreements NA17OAR4320101 and NA22OAR4320151.
 317 We thank Dr. James Russell III for his support and encouragement as an advisor at HU,
 318 and thank National Center for Atmospheric Research (NCAR) Atmospheric Chemistry
 319 Observations & Modeling (ACOM) for hosting WY’s visit during this work. NCAR is
 320 sponsored by the U.S. National Science Foundation (NSF). WACCM is a component of
 321 the Community Earth System Model (CESM), which is supported by NSF and the Of-
 322 fice of Science of the U.S. Department of Energy. Computing resources for the results
 323 presented here were provided by NCAR’s Climate Simulation Laboratory, sponsored by

324 NSF and other agencies, and enabled by the computational and storage resources of NCAR's
 325 Computational and Information Systems Laboratory (CISL).

326 References

- 327 Andrews, D. G., Holton, J. R., & Leovy, C. B. (1987). *Middle atmosphere dynam-*
 328 *ics. no. 40. academic press, 1987.* Academic Press.
- 329 Carn, S. A., Krotkov, N. A., Fisher, B. L., & Li, C. (2022). Out of the blue: Vol-
 330 canic so2 emissions during the 2021–2022 eruptions of hunga tonga—hunga
 331 ha’apai (tonga). *Frontiers in Earth Science, 10*. Retrieved from [https://](https://www.frontiersin.org/articles/10.3389/feart.2022.976962)
 332 www.frontiersin.org/articles/10.3389/feart.2022.976962 doi:
 333 10.3389/feart.2022.976962
- 334 Coy, L., Newman, P. A., Wargan, K., Partyka, G., Strahan, S. E., & Pawson, S.
 335 (2022). Stratospheric circulation changes associated with the hunga tonga-
 336 hunga ha’apai eruption. *Geophysical Research Letters, 49*(22), e2022GL100982.
 337 Retrieved from [https://onlinelibrary.wiley.com/doi/abs/10.1029/](https://onlinelibrary.wiley.com/doi/abs/10.1029/2022GL100982)
 338 [2022GL100982](https://onlinelibrary.wiley.com/doi/abs/10.1029/2022GL100982) doi: 10.1029/2022GL100982
- 339 Dawkins, E. C., Feofilov, A., Rezac, L., Kutepov, A. A., Janches, D., Höffner, J., ...
 340 Russell, J. (2018). Validation of saber v2.0 operational temperature data with
 341 ground-based lidars in the mesosphere-lower thermosphere region (75–105 km).
 342 *Journal of Geophysical Research: Atmospheres, 123*(17), 9916–9934. doi:
 343 10.1029/2018JD028742
- 344 Dunkerton, T. (1978, 12 1). On the mean meridional mass motions of the strato-
 345 sphere and mesosphere. *Journal of the Atmospheric Sciences, 35*(12), 2325–
 346 2333. Retrieved from [https://journals.ametsoc.org/view/journals/](https://journals.ametsoc.org/view/journals/atsc/35/12/1520-0469_1978_035_2325_otmmmm_2_0_co_2.xml)
 347 [atsc/35/12/1520-0469_1978_035_2325_otmmmm_2_0_co_2.xml](https://journals.ametsoc.org/view/journals/atsc/35/12/1520-0469_1978_035_2325_otmmmm_2_0_co_2.xml) doi: 10.1175/
 348 1520-0469(1978)035{\textless}2325:OTMMMM{\textgreater}2.0.CO;2
- 349 Garcia, R. R., & Solomon, S. (1985). The effect of breaking gravity waves
 350 on the dynamics and chemical composition of the mesosphere and lower
 351 thermosphere. *Journal of Geophysical Research, 90*(D2), 3850. Re-
 352 trieved from <http://doi.wiley.com/10.1029/JD090iD02p03850> doi:
 353 10.1029/JD090iD02p03850
- 354 García-Comas, M., López-Puertas, M., Marshall, B. T., Wintersteiner, P. P., Funke,
 355 B., Bermejo-Pantaleón, D., ... Russell III, J. M. (2008). Errors in sounding
 356 of the atmosphere using broadband emission radiometry (saber) kinetic tem-
 357 perature caused by non-local-thermodynamic-equilibrium model parameters.
 358 *Journal of Geophysical Research: Atmospheres, 113*(D24). Retrieved from
 359 <https://onlinelibrary.wiley.com/doi/abs/10.1029/2008JD010105> doi:
 360 10.1029/2008JD010105
- 361 Gettelman, A., Mills, M. J., Kinnison, D. E., Garcia, R. R., Smith, A. K., Marsh,
 362 D. R., ... Randel, W. J. (2019). The whole atmosphere community climate
 363 model version 6 (waccm6). *Journal of Geophysical Research: Atmospheres,*
 364 *124*(23), 12380–12403. doi: 10.1029/2019JD030943
- 365 Harvey, V. L., Pedatella, N., Becker, E., & Randall, C. (2022, 8 16). Evaluation
 366 of polar winter mesopause wind in waccmx+dart. *Journal of Geophysical Re-*
 367 *search: Atmospheres, 127*(15). Retrieved from [https://onlinelibrary.wiley](https://onlinelibrary.wiley.com/doi/10.1029/2022JD037063)
 368 [.com/doi/10.1029/2022JD037063](https://onlinelibrary.wiley.com/doi/10.1029/2022JD037063) doi: 10.1029/2022JD037063
- 369 Holton, J. R. (1983, 10 1). The influence of gravity wave breaking on the general
 370 circulation of the middle atmosphere. *Journal of the Atmospheric Sciences,*
 371 *40*(10), 2497–2507. Retrieved from [https://journals.ametsoc.org/view/](https://journals.ametsoc.org/view/journals/atsc/40/10/1520-0469_1983_040_2497_tiogwb_2_0_co_2.xml)
 372 [journals/atsc/40/10/1520-0469_1983_040_2497_tiogwb_2_0_co_2.xml](https://journals.ametsoc.org/view/journals/atsc/40/10/1520-0469_1983_040_2497_tiogwb_2_0_co_2.xml) doi:
 373 10.1175/1520-0469(1983)040<2497:TIOGWB>2.0.CO;2
- 374 Holton, J. R. (2004). *An introduction to dynamic meteorology* (4th ed.; R. Dmowska
 375 & J. R. Holton, Eds.). Burlington, MA: Elsevier Academic Press,. Retrieved
 376 from <http://books.google.com/books?id=fhW5oDv3EPsC>

- 377 Holton, J. R., & Mass, C. (1976, 11 1). Stratospheric vacillation cycles. *Journal*
378 *of the Atmospheric Sciences*, *33*(11), 2218–2225. Retrieved from [https://](https://journals.ametsoc.org/view/journals/atasc/33/11/1520-0469_1976_033_2218_svc_2.0_co_2.xml)
379 [journals.ametsoc.org/view/journals/atasc/33/11/1520-0469_1976_033](https://journals.ametsoc.org/view/journals/atasc/33/11/1520-0469_1976_033_2218_svc_2.0_co_2.xml)
380 [_2218_svc_2.0_co_2.xml](https://journals.ametsoc.org/view/journals/atasc/33/11/1520-0469_1976_033_2218_svc_2.0_co_2.xml) doi: 10.1175/1520-0469(1976)033{\textless}2218:
381 SVC{\textgreater}2.0.CO;2
- 382 Khaykin, S., Podglajen, A., Ploeger, F., Grooß, J.-U., Tence, F., Bekki, S., ...
383 Ravetta, F. (2022, 12 14). Global perturbation of stratospheric water and
384 aerosol burden by hunga eruption. *Communications Earth & Environ-*
385 *ment*, *3*(1), 1–15. Retrieved from [https://www.nature.com/articles/](https://www.nature.com/articles/s43247-022-00652-x)
386 [s43247-022-00652-x](https://www.nature.com/articles/s43247-022-00652-x) doi: 10.1038/s43247-022-00652-x
- 387 Lindzen, R. S. (1981). Turbulence and stress owing to gravity wave and
388 tidal breakdown. *Journal of Geophysical Research*, *86*(C10), 9707. Re-
389 trieved from <http://doi.wiley.com/10.1029/JC086iC10p09707> doi:
390 [10.1029/JC086iC10p09707](http://doi.wiley.com/10.1029/JC086iC10p09707)
- 391 Livesey, N. J., Read, W., Lambert, A., Cofield, R., Cuddy, D., Froidevaux, L., ...
392 Co, R. E. (2020). *Earth observing system (eos) aura microwave limb sounder*
393 *(mls) description document* (Tech. Rep.).
- 394 Millán, L., Santee, M. L., Lambert, A., Livesey, N. J., Werner, F., Schwartz, M. J.,
395 ... Froidevaux, L. (2022). The hunga tonga-hunga ha’apai hydration of the
396 stratosphere. *Geophysical Research Letters*, *49*(13), e2022GL099381. Retrieved
397 from <http://onlinelibrary.wiley.com/doi/abs/10.1029/2022GL099381>
398 doi: 10.1029/2022GL099381
- 399 Mlynczak, M. G., Daniels, T., Hunt, L. A., Yue, J., Marshall, B. T., Russell, J. M.,
400 ... Yee, J. H. (2020). Radiometric stability of the saber instrument. *Earth and*
401 *Space Science*, *7*(2), e2019EA001011. doi: 10.1029/2019EA001011
- 402 Mlynczak, M. G., Marshall, B. T., Garcia, R. R., Hunt, L., Yue, J., Harvey, V. L.,
403 ... Russell, J. (2023, 3 16). Algorithm stability and the long-term geospace
404 data record from timed/saber. *Geophysical Research Letters*, *50*(5). Retrieved
405 from <https://onlinelibrary.wiley.com/doi/10.1029/2022GL102398> doi:
406 [10.1029/2022GL102398](https://onlinelibrary.wiley.com/doi/10.1029/2022GL102398)
- 407 Proud, S. R., Prata, A. T., & Schmauß, S. (2022, 11 4). The january 2022 erup-
408 tion of hunga tonga-hunga ha’apai volcano reached the mesosphere. *Science*,
409 *378*(6619), 554–557. Retrieved from [http://www.science.org/doi/10.1126/](http://www.science.org/doi/10.1126/science.abo4076)
410 [science.abo4076](http://www.science.org/doi/10.1126/science.abo4076) doi: 10.1126/science.abo4076
- 411 Randall, C. E., Harvey, V. L., Siskind, D. E., France, J., Bernath, P. F., Boone,
412 C. D., & Walker, K. A. (2009). Nox descent in the arctic middle atmo-
413 sphere in early 2009. *Geophysical Research Letters*, *36*(18). Retrieved from
414 <https://onlinelibrary.wiley.com/doi/abs/10.1029/2009GL039706> doi:
415 [10.1029/2009GL039706](https://onlinelibrary.wiley.com/doi/abs/10.1029/2009GL039706)
- 416 Randel, W. J., Johnston, B. R., Braun, J. J., Sokolovskiy, S., Vömel, H., Podglajen,
417 A., & Legras, B. (2023, 1). Stratospheric water vapor from the hunga
418 tonga–hunga ha’apai volcanic eruption deduced from cosmic-2 radio occul-
419 tation. *Remote Sensing*, *15*(8), 2167. Retrieved from [https://www.mdpi.com/](https://www.mdpi.com/2072-4292/15/8/2167)
420 [2072-4292/15/8/2167](https://www.mdpi.com/2072-4292/15/8/2167) doi: 10.3390/rs15082167
- 421 Randel, W. J., & Newman, P. A. (1998). The stratosphere in the southern hemi-
422 sphere. In D. J. Karoly & D. G. Vincent (Eds.), *Meteorology of the southern*
423 *hemisphere* (pp. 243–282). Boston, MA: American Meteorological Society. Re-
424 trieved from https://doi.org/10.1007/978-1-935704-10-2_9
- 425 Remsberg, E., Marshall, B. T., Garcia-Comas, M., Krueger, D., Lingenfelter, G. S.,
426 Martin-Torres, J., ... Thompson, R. E. (2008). Assessment of the quality of
427 the version 1.07 temperature-versus-pressure profiles of the middle atmosphere
428 from timed/saber. *Journal of Geophysical Research: Atmospheres*, *113*(D17),
429 17101. doi: 10.1029/2008JD010013
- 430 Rienecker, M., Suarez, M., Todling, R., Bacmeister, J., Takacs, L., Liu, H.-C., ...
431 Nielsen, J. (2018). *The geos-5 data assimilation system— documentation of*

- versions 5.0.1, 5.1.0, and 5.2.0 (Tech. Rep.).
- Russell, J. M., Mlynczak, M. G., Gordley, L. L., Tansock, J. J., Jr., & Esplin, R. W. (1999, 10 20). Overview of the saber experiment and preliminary calibration results. In (Vol. 3756, p. 277). International Society for Optics and Photonics. Retrieved from <https://www.spiedigitallibrary.org/conference-proceedings-of-spie/3756/0000/Overview-of-the-SABER-experiment-and-preliminary-calibration-results/10.1117/12.366382.full> doi: 10.1117/12.366382
- Schoeberl, M. R., Wang, Y., Ueyama, R., Taha, G., Jensen, E., & Yu, W. (2022). Analysis and impact of the hunga tonga-hunga ha'apai stratospheric water vapor plume. *Geophysical Research Letters*, *49*(20), e2022GL100248. Retrieved from <https://onlinelibrary.wiley.com/doi/abs/10.1029/2022GL100248> doi: 10.1029/2022GL100248
- Sellitto, P., Podglajen, A., Belhadji, R., Boichu, M., Carboni, E., Cuesta, J., ... Legras, B. (2022, 11 19). The unexpected radiative impact of the hunga tonga eruption of 15th january 2022. *Communications Earth & Environment*, *3*(1), 1–10. Retrieved from <http://www.nature.com/articles/s43247-022-00618-z> doi: 10.1038/s43247-022-00618-z
- Smith, A. K., Garcia, R. R., Marsh, D. R., & Richter, J. H. (2011, 10 20). Waccm simulations of the mean circulation and trace species transport in the winter mesosphere. *Journal of Geophysical Research*, *116*(D20), D20115. Retrieved from <http://doi.wiley.com/10.1029/2011JD016083> doi: 10.1029/2011JD016083
- Smith, A. K., Marsh, D. R., Mlynczak, M. G., & Mast, J. C. (2010). Temporal variations of atomic oxygen in the upper mesosphere from saber. *Journal of Geophysical Research: Atmospheres*, *115*(D18). Retrieved from <https://onlinelibrary.wiley.com/doi/abs/10.1029/2009JD013434> doi: 10.1029/2009JD013434
- Smith, A. K., Pedatella, N. M., & Mullen, Z. K. (2020, 3 1). Interhemispheric coupling mechanisms in the middle atmosphere of waccm6. *Journal of the Atmospheric Sciences*, *77*(3), 1101–1118. Retrieved from <https://journals.ametsoc.org/view/journals/atsc/77/3/jas-d-19-0253.1.xml> doi: 10.1175/JAS-D-19-0253.1
- Taha, G., Loughman, R., Colarco, P. R., Zhu, T., Thomason, L. W., & Jaross, G. (2022). Tracking the 2022 hunga tonga-hunga ha'apai aerosol cloud in the upper and middle stratosphere using space-based observations. *Geophysical Research Letters*, *49*(19), e2022GL100091. Retrieved from <http://onlinelibrary.wiley.com/doi/abs/10.1029/2022GL100091> doi: 10.1029/2022GL100091
- Vincent, R. A. (2015, 3). The dynamics of the mesosphere and lower thermosphere: a brief review. *Progress in Earth and Planetary Science*, *2*(1), 4. Retrieved from <http://www.progearthplanetosci.com/content/2/1/4> doi: 10.1186/s40645-015-0035-8
- Vömel, H., Evan, S., & Tully, M. (2022, 9 23). Water vapor injection into the stratosphere by hunga tonga-hunga ha'apai. *Science*, *377*(6613), 1444–1447. Retrieved from <https://www.science.org/doi/full/10.1126/science.abq2299> doi: 10.1126/science.abq2299
- Wang, X., Randel, W., Zhu, Y., Tilmes, S., Starr, J., Yu, W., ... Li, J. (2022, 11 26). *Stratospheric climate anomalies and ozone loss caused by the hunga tonga volcanic eruption* (Tech. Rep.). Retrieved from <https://essopenarchive.org/doi/full/10.1002/essoar.10512922.1>
- Waters, J. W., Froidevaux, L., Harwood, R. S., Jarnot, R. F., Pickett, H. M., Read, W. G., ... Walch, M. J. (2006, 5). The earth observing system microwave limb sounder (eos mls) on the aura satellite. *IEEE Transactions on Geoscience and Remote Sensing*, *44*(5), 1075–1092. doi: 10.1109/TGRS.2006.873771

- 487 Wehrbein, W. M., & Leovy, C. B. (1982, 7 1). An accurate radiative heat-
488 ing and cooling algorithm for use in a dynamical model of the middle at-
489 mosphere. *Journal of the Atmospheric Sciences*, 39(7), 1532–1544. Re-
490 trieved from [https://journals.ametsoc.org/view/journals/atsc/](https://journals.ametsoc.org/view/journals/atsc/39/7/1520-0469_1982_039_1532_aarhac_2_0_co_2.xml)
491 [39/7/1520-0469_1982_039_1532_aarhac_2_0_co_2.xml](https://journals.ametsoc.org/view/journals/atsc/39/7/1520-0469_1982_039_1532_aarhac_2_0_co_2.xml) doi: 10.1175/
492 1520-0469(1982)039<>1532:AARHAC<>2.0.CO;2
- 493 Zhu, Y., Bardeen, C. G., Tilmes, S., Mills, M. J., Wang, X., Harvey, V. L., ... Toon,
494 O. B. (2022, 10 22). Perturbations in stratospheric aerosol evolution due to the
495 water-rich plume of the 2022 hunga-tonga eruption. *Communications Earth &*
496 *Environment*, 3(1), 1–7. Retrieved from [https://www.nature.com/articles/](https://www.nature.com/articles/s43247-022-00580-w)
497 [s43247-022-00580-w](https://www.nature.com/articles/s43247-022-00580-w) doi: 10.1038/s43247-022-00580-w

Figure1.

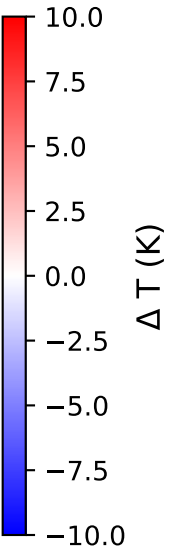
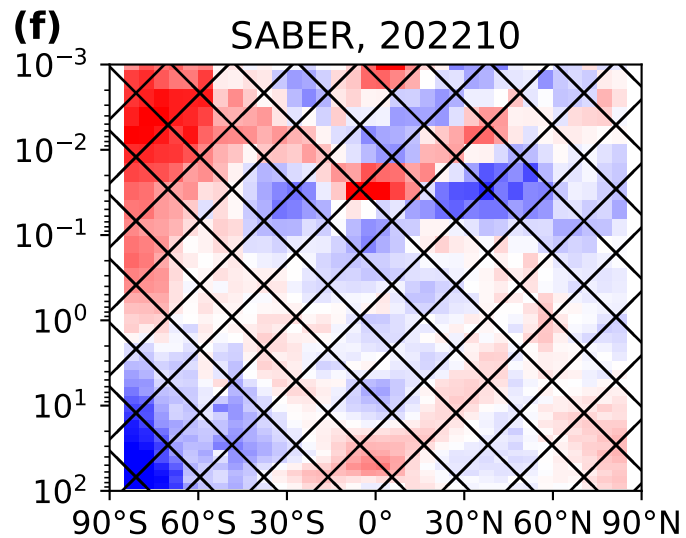
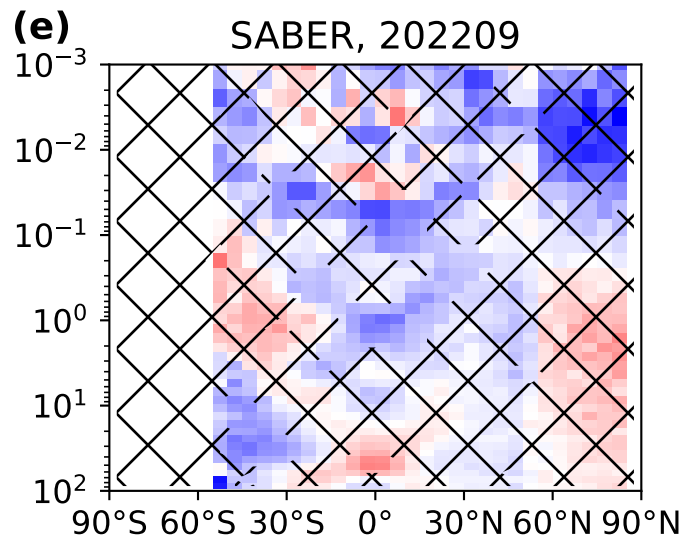
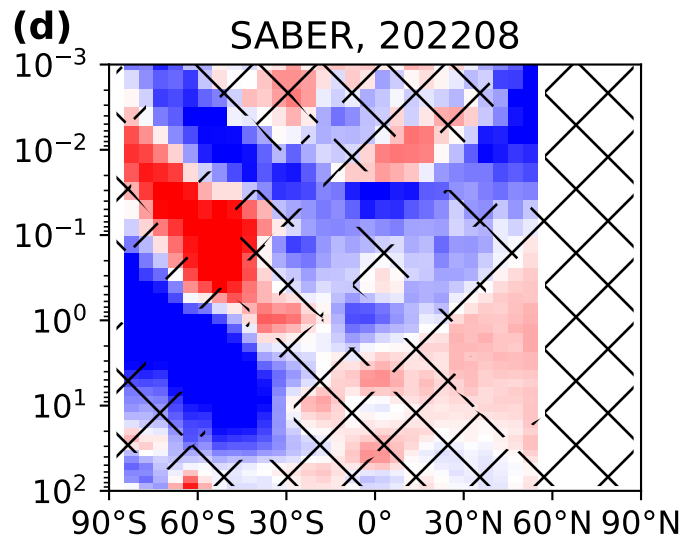
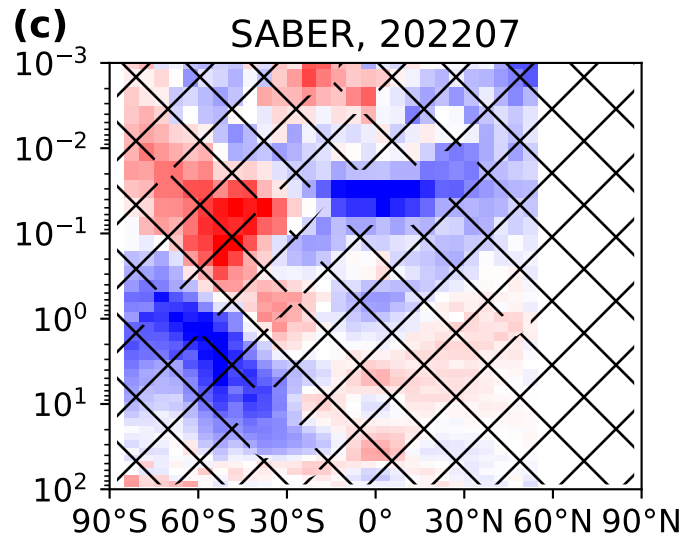
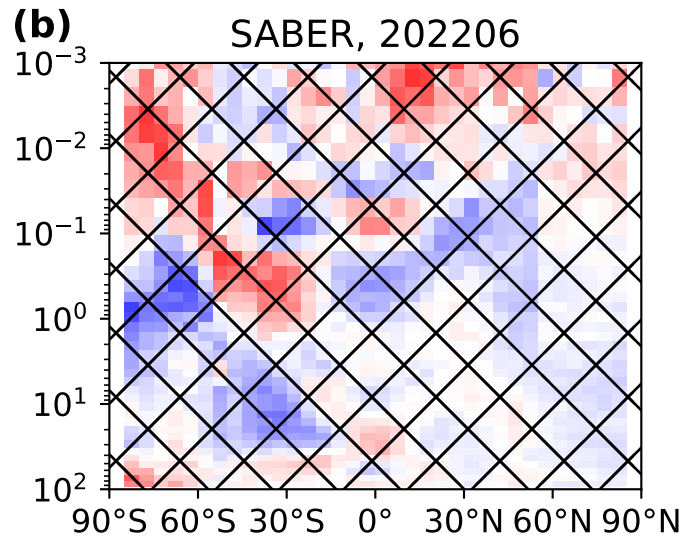
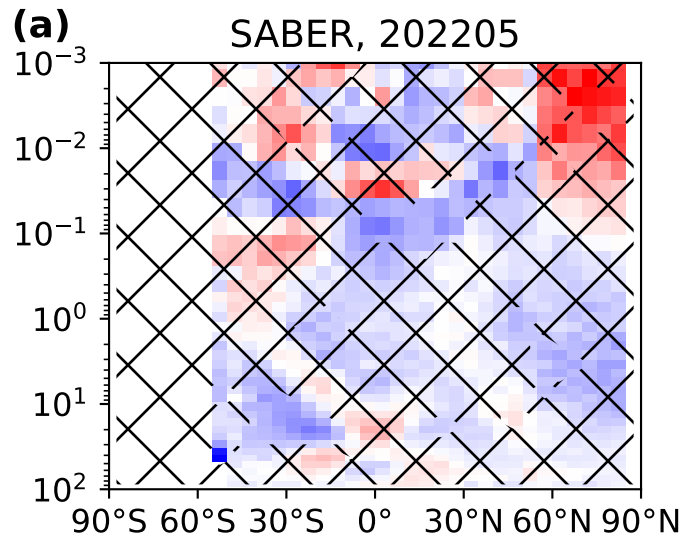


Figure2.

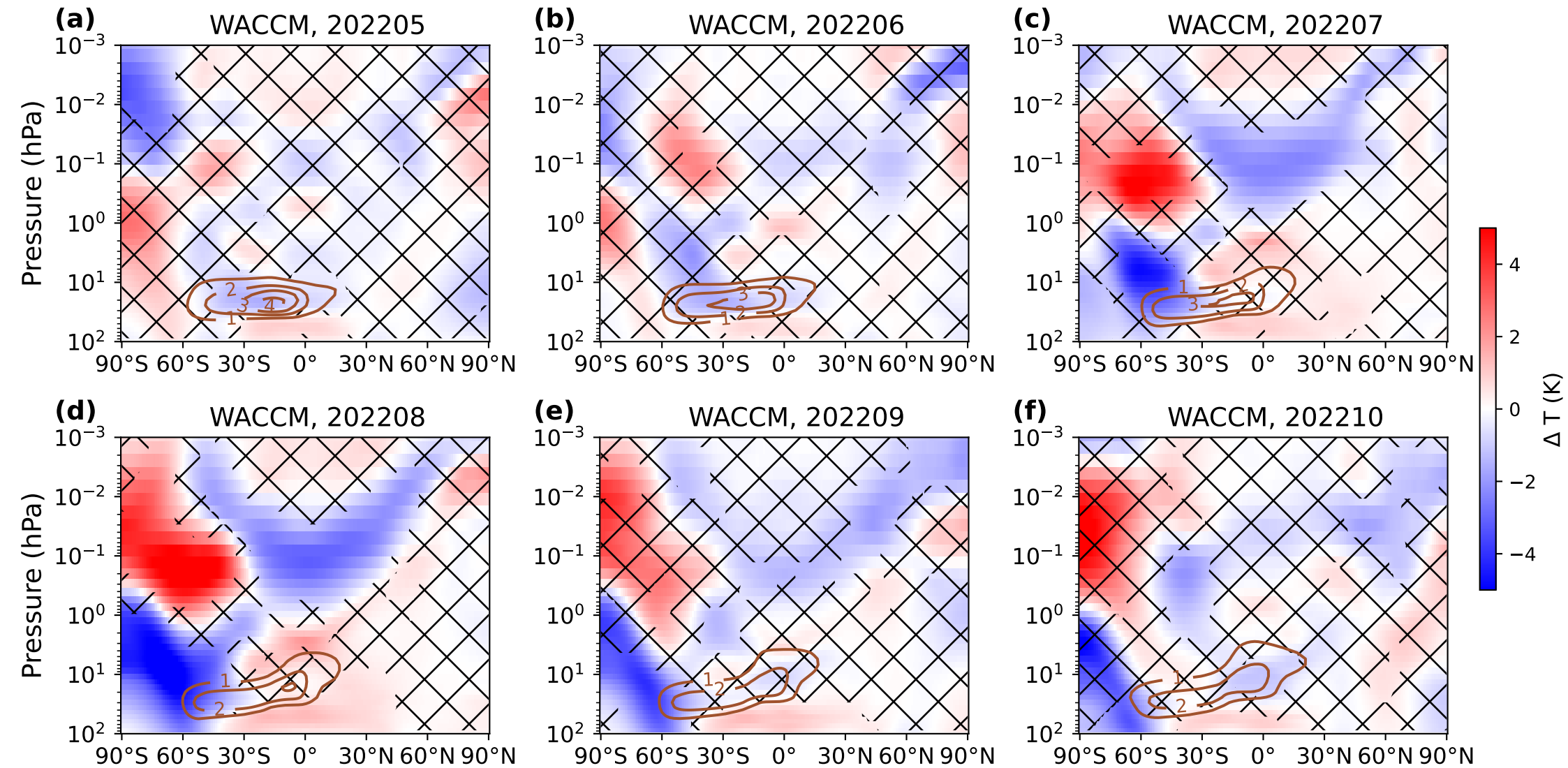


Figure3.

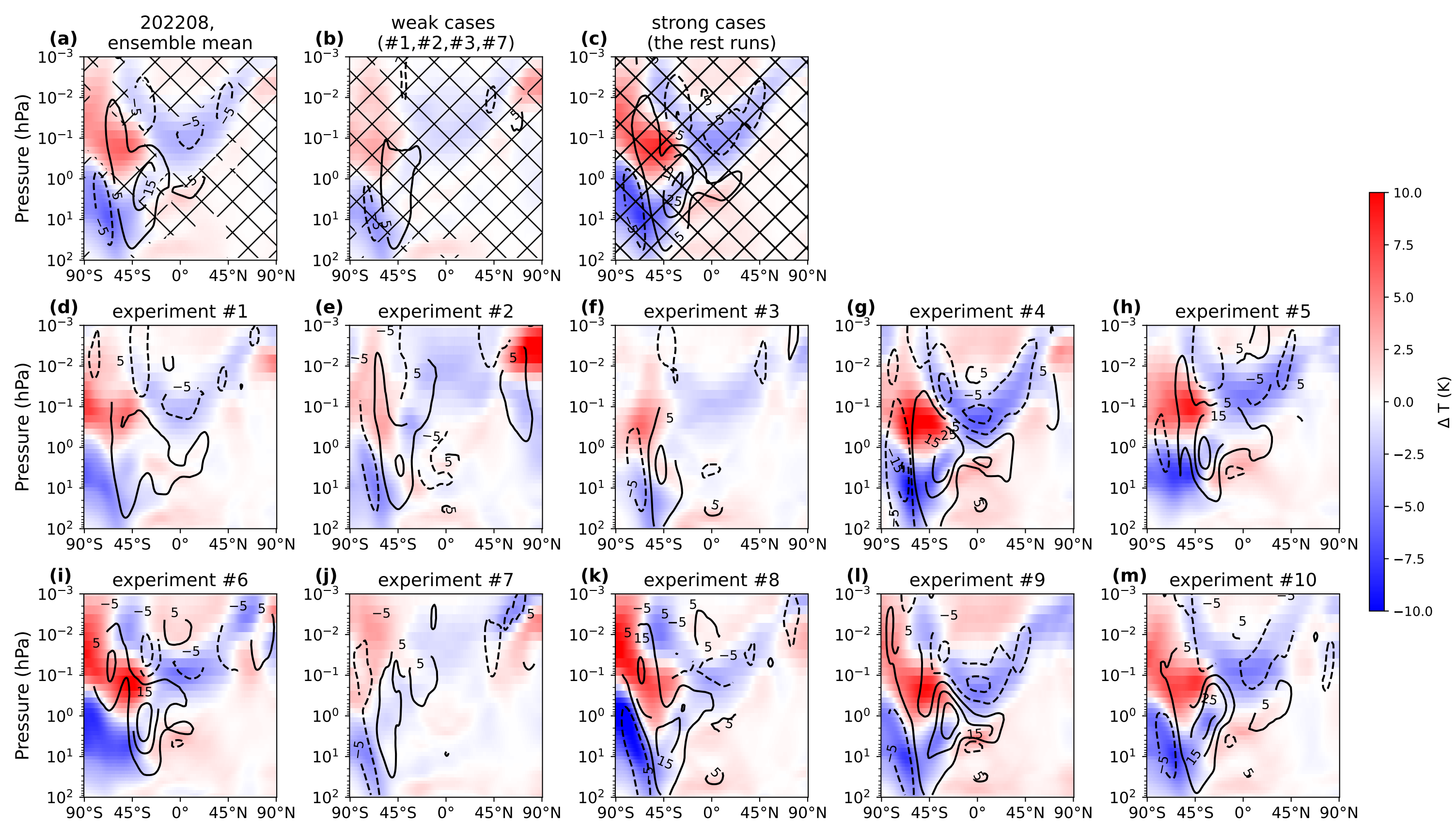


Figure4.

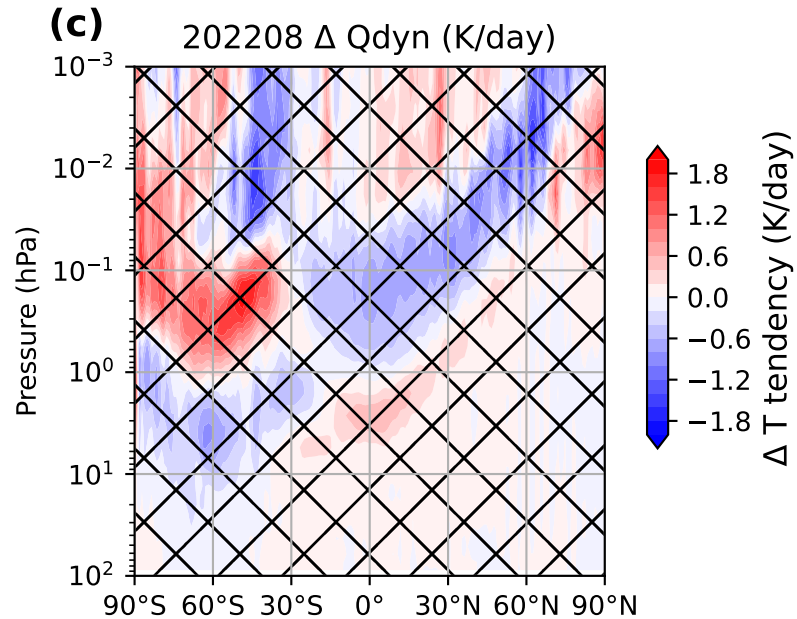
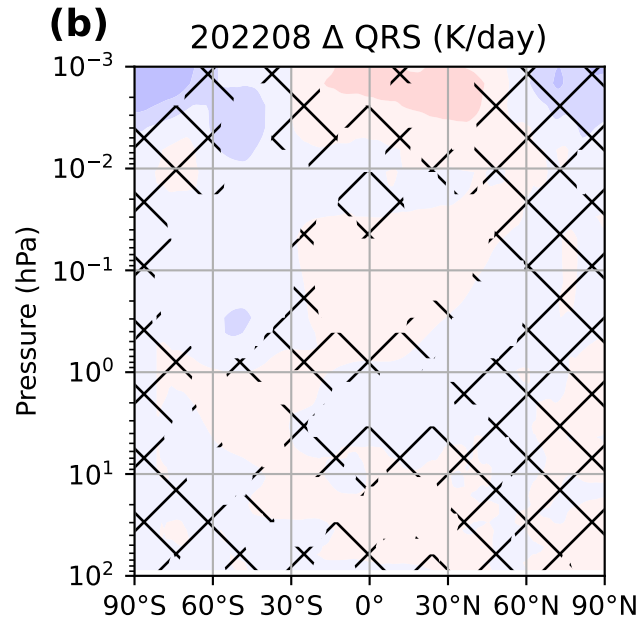
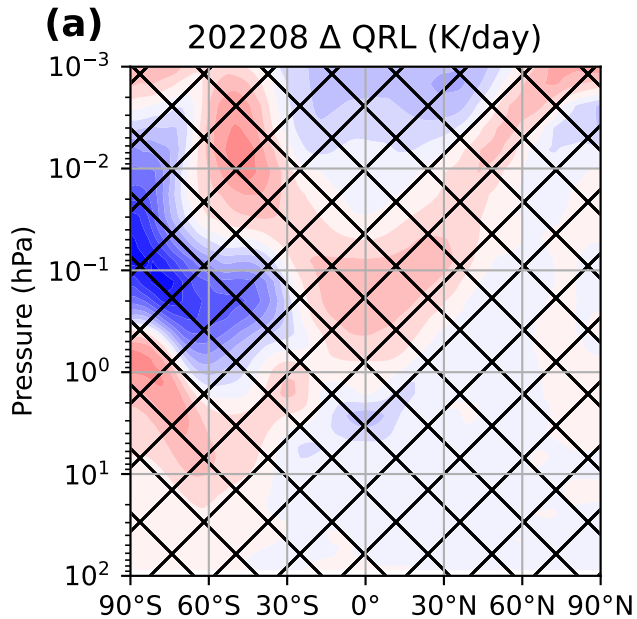
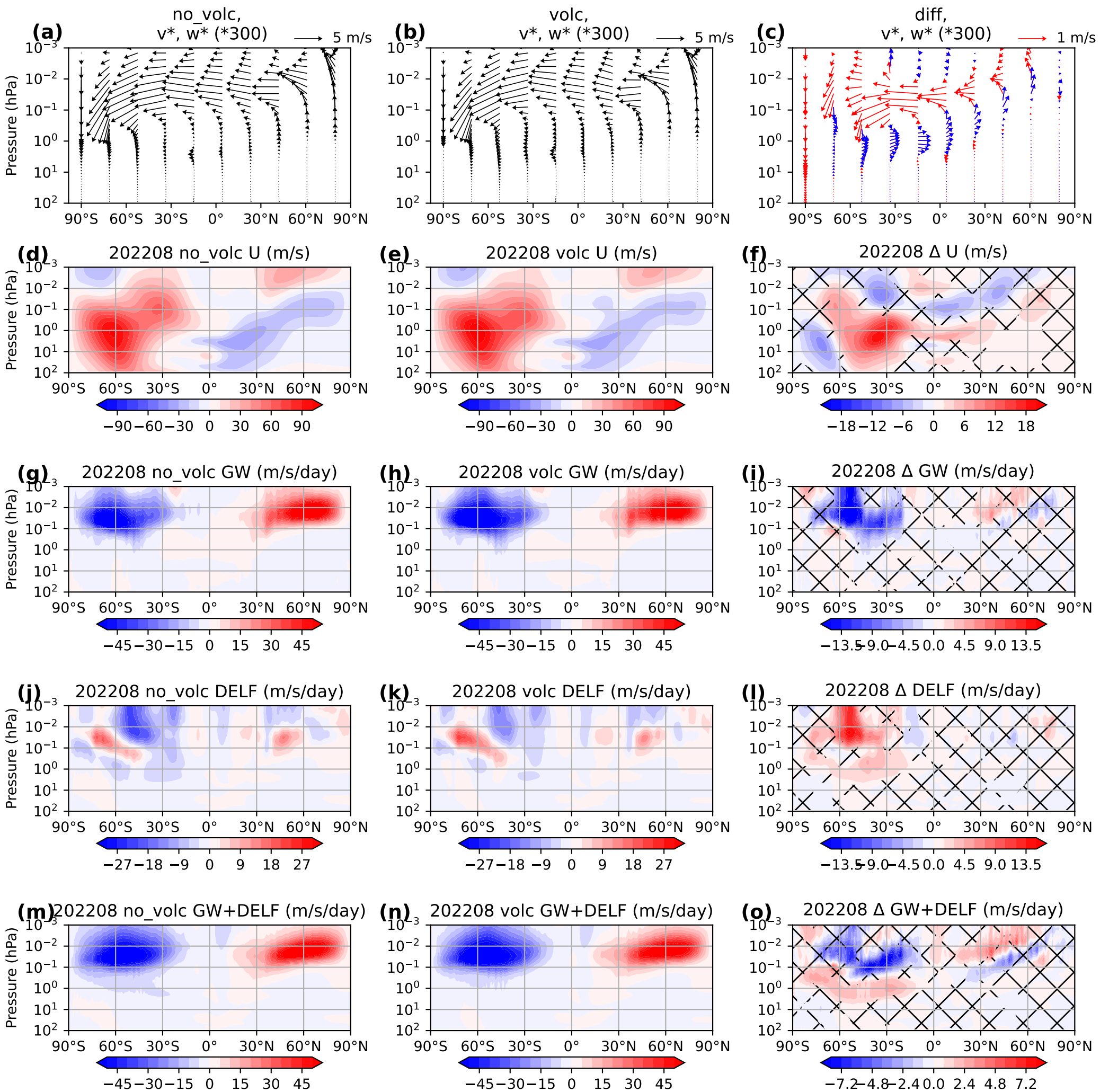


Figure 5.



Mesospheric temperature and circulation response to the Hunga Tonga-Hunga-Ha'apai volcanic eruption

Wandi Yu¹, Rolando R. Garcia², Jia Yue^{3,4}, Anne K. Smith², Xinyue Wang², William J. Randel², Zishun Qiao⁵, Yunqian Zhu^{6,7}, V.Lynn Harvey^{6,8}, Simone Tilmes², Martin G. Mlynczak⁹

¹Department of Atmospheric and Planetary Sciences, Hampton University, Hampton, VA, USA

²Atmospheric Chemistry Observations & Modeling, National Center for Atmospheric Research, Boulder, CO, USA

³NASA Goddard Space Flight Center, Greenbelt, MD, USA

⁴Catholic University of America, Washington, DC, USA

⁵Embry-Riddle Aeronautical University, FL, USA

⁶Laboratory for Atmospheric and Space Physics, University of Colorado Boulder, Boulder, USA

⁷University of Colorado Cooperative Institute for Research in Environmental Sciences (CIRES) at the

NOAA Chemical Sciences Laboratory, Boulder, CO, USA

⁸Atmospheric and Oceanic Sciences Department, University of Colorado, Boulder, CO, USA

⁹NASA Langley Research Center, Hampton, VA, USA

Key Points:

- SABER observed unprecedented mesospheric temperature variations in the Southern Hemisphere in August 2022 after the HTHH eruption.
- WACCM simulations indicate that changes in the mesospheric temperature are due to a stronger mesospheric meridional circulation.
- Stronger stratospheric westerlies after eruption enhance westward gravity wave drag in the mesosphere, thus a stronger circulation.

Corresponding author: Wandu Yu, wandi.yu@hamptonu.edu

Abstract

The Hunga Tonga Hunga-Ha’apai (HTHH) volcanic eruption on 15 January 2022 injected water vapor and SO_2 into the stratosphere. Several months after the eruption, significantly stronger westerlies, and a weaker Brewer-Dobson circulation developed in the stratosphere of the Southern Hemisphere and were accompanied by unprecedented temperature anomalies in the stratosphere and mesosphere. In August 2022 the Sounding of the Atmosphere using Broadband Emission Radiometry (SABER) satellite instrument observed record-breaking temperature anomalies in the stratosphere and mesosphere that alternate signs with altitude. Ensemble simulations carried out with the Whole Atmosphere Community Climate Model (WACCM6) indicate that the strengthening of the stratospheric westerlies explains the mesospheric temperature changes. The stronger westerlies cause stronger westward gravity wave drag in the mesosphere, accelerating the mesospheric mean meridional circulation. The stronger mesospheric circulation, in turn, plays a dominant role in driving the changes in mesospheric temperatures. This study highlights the impact of large volcanic eruptions on middle atmospheric dynamics and provides insight into their long-term effects in the mesosphere. On the other hand, we could not discern a clear mechanism for the observed changes in stratospheric circulation. In fact, an examination of the WACCM ensemble reveals that not every member reproduces the large changes observed by SABER. We conclude that there is a stochastic component to the stratospheric response to the HTHH eruption.

Plain Language Summary

This work studies the impact of the Hunga Tonga-Hunga Ha’apai volcanic eruption, which took place on January 15, 2022, on the earth’s mesosphere (55 km – 80 km). The eruption injected water vapor and SO_2 into the stratosphere, which was followed by changes in the wind patterns in the stratosphere (16 km – 55 km). Concurrent with these changes, we observed unprecedented temperature changes in the mesosphere, with record high and low temperature anomalies in August that alternate signs with altitude. We used climate model simulations to show that the changes in stratospheric winds were ultimately responsible for these record-breaking mesospheric temperatures. We found that the stronger winds in the stratosphere enhanced gravity wave breaking in the mesosphere, which led to changes in the circulation and thus the temperature. However, we could not find a clear mechanism for the changes observed in the stratosphere.

1 Introduction

On 15 January 2022, a submarine volcano erupted in Hunga Tonga - Hunga Ha’apai (HTHH, 20.54°S, 175.38°W). The volcanic plume reached 55-57 km (Carn et al., 2022; Proud et al., 2022). This eruption injected ~ 50 -150 Tg of water vapor into the stratosphere and increased the total stratospheric water vapor burden by 5-13% reported by different observational instruments (Khaykin et al., 2022; Millán et al., 2022; Randel et al., 2023; Vömel et al., 2022) Meanwhile, 0.4-0.5 Tg of SO_2 was also injected into the stratosphere (Carn et al., 2022), and formed sulfate aerosols (Khaykin et al., 2022; Taha et al., 2022; Zhu et al., 2022).

The HTHH volcanic eruption changed the dynamics in the stratosphere. In the few months following the eruption, the injected water vapor cooled the middle stratosphere and warmed the lower stratosphere; and the sulfate aerosol formed from the injected SO_2 warmed the lower stratosphere (Schoeberl et al., 2022; Sellitto et al., 2022; Wang et al., 2022). These warming and cooling patterns coincide with the distribution of water vapor and sulfate aerosol. However, in the austral winter of 2022, the stratospheric westerly jet shifted equatorward and strengthened, concurrent with a weakening of the stratospheric Brewer-Dobson circulation (Coy et al., 2022; Wang et al., 2022), leading to a depletion of ozone in the mid-latitudes (Wang et al., 2022). At this time, the temperature

74 anomalies consistent with the changes in the stratospheric jet no longer coincided with
75 the location of the water vapor and aerosol anomalies.

76 The mesosphere is the layer of the atmosphere above the stratosphere, from ~ 50
77 km to ~ 85 km, or about 1 hPa to 0.01 hPa. The mesospheric temperature can be en-
78 visaged as being composed of the global mean vertical profile, determined by radiative
79 equilibrium, plus local departures determined mainly by dynamical processes (Andrews
80 et al., 1987). The mesospheric meridional circulation is the most important dynamical
81 process that transports heat and chemical species (Randall et al., 2009; Smith et al., 2011,
82 2010). It is composed of a single, inter-hemispheric cell, with ascent in the summer hemi-
83 sphere and descent in the winter hemisphere, connected by cross-equatorial flow from
84 the summer hemisphere to the winter hemisphere. The circulation is strongest near the
85 two solstices (Dunkerton, 1978). Gravity waves propagating from below, some filtered
86 out by the winds in the stratosphere, break in the mesosphere and deposit angular mo-
87 mentum that drives the mesospheric circulation (Andrews et al., 1987; Garcia & Solomon,
88 1985; Holton, 1983; Lindzen, 1981; Vincent, 2015). The gravity wave breaking that drives
89 the mean meridional circulation is also referred to as “gravity wave drag”.

90 The present study examines the impact of the HTHH volcanic eruption on the mid-
91 dle atmosphere, focusing specifically on changes in temperature and circulation in the
92 mesosphere. By analyzing both satellite observations and model simulations, we aim to
93 address several scientific questions. These include: (1) How does the mesospheric tem-
94 perature respond to the HTHH volcanic eruption? (2) What is the relationship between
95 changes in temperature and the mesospheric circulation that follow the eruption? and
96 (3) What mechanisms contribute to the changes in mesospheric circulation following the
97 eruption? We also discuss our attempts to understand the changes in stratospheric dy-
98 namics following the eruption, whose origin remains unclear.

99 2 Data and Model

100 The Sounding of the Atmosphere using Broadband Emission Radiometry (SABER)
101 instrument onboard NASA’s TIMED (Thermosphere Ionosphere Mesosphere Energet-
102 ics Dynamics) satellite has been measuring temperature and chemical species in the mid-
103 dle atmosphere since January 2002 (Russell et al., 1999). To prevent the SABER detec-
104 tor from pointing directly at the Sun, TIMED performs a “yaw maneuver” that switches
105 coverage from $83^{\circ}\text{S} - 53^{\circ}\text{N}$ to $83^{\circ}\text{N} - 53^{\circ}\text{S}$ every 60 days. SABER temperature data was
106 validated by Dawkins et al. (2018), García-Comas et al. (2008), and Remsberg et al. (2008),
107 and the stability of SABER calibration was examined by Mlynczak et al. (2020). The
108 SABER temperature product covers the altitude range from the tropopause (~ 17 km)
109 to 110 km. In the mesosphere, the SABER temperature product has a vertical resolu-
110 tion of about 2 km, and we grid it into 5° latitude by 10° longitude bins. We use v2.07
111 of the SABER temperature product before December 2019, and v2.08 thereafter (Mlynczak
112 et al., 2023). We use SABER temperature from 2003 to 2022, to avoid the possibility
113 of errors due to the icing on the detector in the first year of operation (Remsberg et al.,
114 2008).

115 We use NCAR’s Whole Atmosphere Community Climate Model (WACCM6; Get-
116 telman et al., 2019) to analyze the dynamic response of the stratosphere and mesosphere
117 to volcanic eruption. This version of WACCM has 70 vertical layers and a horizontal res-
118 olution of 0.95° latitude by 1.25° longitude. We carried out two sets of experiments, each
119 with 10 ensemble members. In the control ensemble, we nudge the temperature and wind
120 field to the GEOS5 meteorological analysis data (Rienecker et al., 2018) throughout Jan-
121 uary 2022 until the beginning of February. The only difference between the ensemble mem-
122 bers is that nudging ends on slightly different dates, in the range from 27 January 2022
123 to 5 February 2022. Once nudging end, the model runs freely and fully coupled to the
124 ocean, sea-ice, and land. The volcanic eruption ensemble applies the same settings as

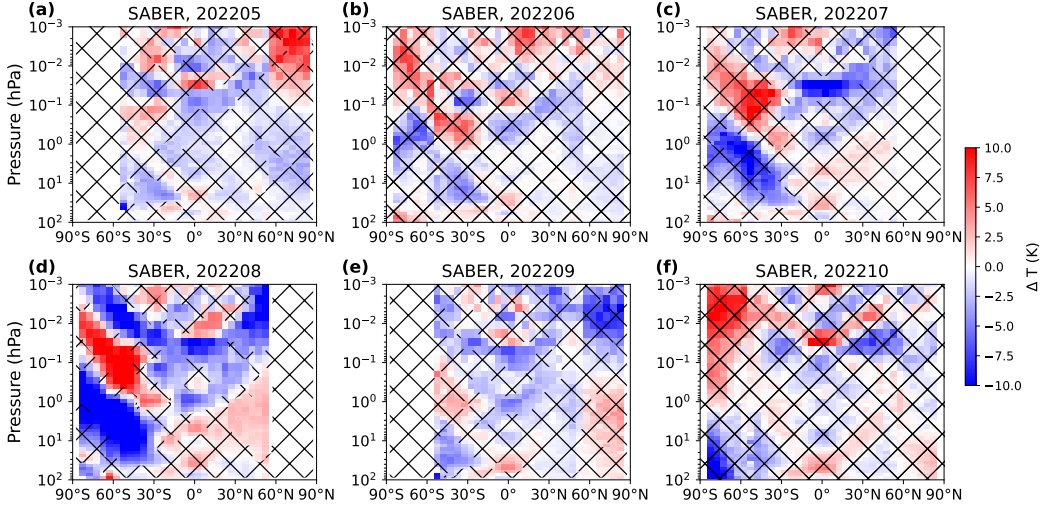


Figure 1. Monthly mean zonal mean temperature anomalies (2022 minus climatology) observed by SABER; the areas without hatching meet two thresholds: (1) must be outside of previous SABER variability and (2) exceed two standard deviations from the climatology. The plots cover the period from May to October 2022.

125 the control group but with the addition of the volcanic forcings. We inject 150 Tg of wa-
 126 ter vapor and 0.42 Tg SO_2 on January 15 following Zhu et al. (2022). Wang et al. (2022)
 127 have already demonstrated that this model setting successfully reproduces satellite ob-
 128 servations of stratospheric dynamics following the HTHH volcanic eruption.

129 3 Results

130 The middle atmospheric temperature observed by SABER in 2022 displayed sig-
 131 nificant anomalies compared to the climatology of the previous 20 years of observations.
 132 Positive and negative anomalies in mesospheric temperature that exceeded both the high
 133 or low values in the historical record and two standard deviations from the climatolog-
 134 ical mean were occasionally observed, as shown in Fig. 1 (areas not covered by hatch-
 135 ing). Some 2022 temperatures can be record-breaking but within 2 sigmas of the clima-
 136 tological mean, while some can exceed the 2-sigma threshold but not be record-breaking.
 137 Thus, we use both criteria jointly as an indication of statistical significance. The peak
 138 temperature anomalies occurred in July and August, revealing a tripolar pattern char-
 139 acterized by a cold center in the Southern Hemisphere (SH) extratropical stratosphere,
 140 a warm center in the mid-latitude mesosphere, and V-shaped cold anomalies extending
 141 from the lower mesosphere in the tropics to the upper mesosphere in the extratropics
 142 in both hemispheres, as shown in Fig. 1c-d. Notably, in August 2022, the mesospheric
 143 temperature in the tripolar structure reached record lows or highs for the entire SABER
 144 era (2003-2022). The August temperature anomalies are as large as ± 10 K in the strato-
 145 sphere and mesosphere. This tripolar structure weakens in September and the signifi-
 146 cant anomalies dissipate after September 2022. We compared SABER temperature anoma-
 147 lies with those from the Microwave Limb Sounder (MLS, Livesey et al., 2020; Waters et
 148 al., 2006) v5.0 temperature product (not shown), which has a better vertical resolution
 149 in the stratosphere and has global coverage but a coarser vertical resolution in the meso-
 150 sphere, and draw the same conclusion.

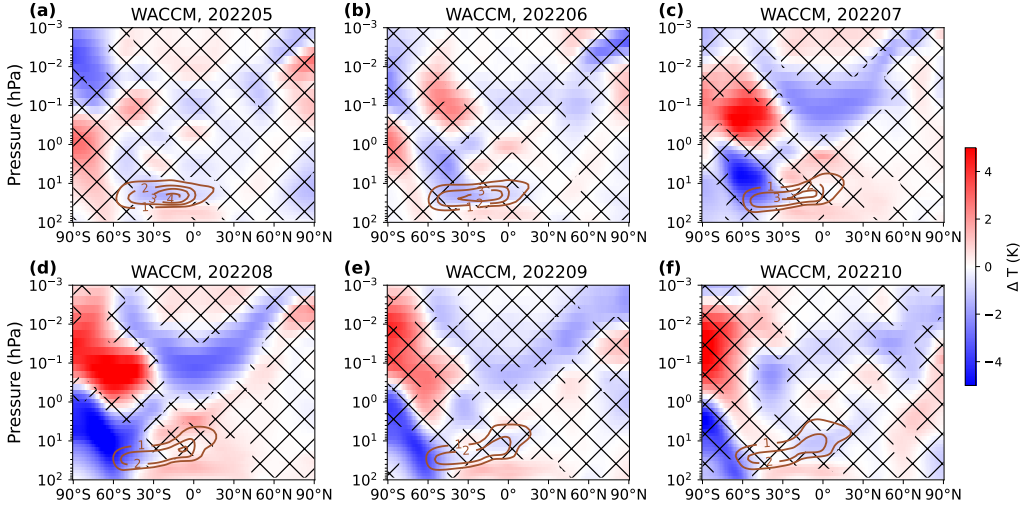


Figure 2. The 10-ensemble mean monthly mean zonal mean temperature difference between the volcano run and the control run in WACCM. The areas with differences that have a p-value > 0.05 in a Student’s t-test are indicated by hatching. The plots cover the period from May to October 2022. Brown contours show zonal mean water vapor mixing ratio anomalies in ppmv.

151 To untangle the influence of the volcanic eruption from internal variability on changes
 152 in mesospheric temperature, we performed WACCM simulations where the only differ-
 153 ence with respect to the control ensemble is whether H_2O and SO_2 are injected. We ran
 154 fully coupled free-running WACCM after February 2022 to capture the interaction be-
 155 tween composition and circulation. In Fig. 2, we show the temperature difference (ΔT)
 156 between the ensemble means of the WACCM volcano case and the control case. The en-
 157 semble mean ΔT (the difference between the volcanic and control ensemble means) in-
 158 creased over time, exhibiting the same significant tripolar structure as that observed by
 159 SABER in July and August, with the structure weakening after September. The mod-
 160 eled ensemble mean ΔT pattern mirrors the observed tripolar structure. The magni-
 161 tude of the ensemble-average signal is, however, 40% of that seen in the observations.

162 We examined the members of the volcanic ensemble individually for August 2022,
 163 comparing each one against the mean of the control ensemble. All ten volcanic ensem-
 164 ble members reproduce the observed temperature anomaly pattern in that month; six
 165 out of ten have an anomaly amplitude comparable to the observations (Figs. 3g-i and
 166 3k-m); and four show a smaller amplitude (Figs. 3d-f and 3j). We refer to the six cases
 167 with a signal amplitude that is comparable to observations as “strong” cases, and to the
 168 other four cases as “weak” cases. The strong and weak cases occur independently of the
 169 date when nudging was stopped. The ensemble mean of the strong cases shows a signif-
 170 icant tripolar structure with magnitudes comparable to the observations, with a max-
 171 imum ΔT of ± 10 K in the stratosphere and mesosphere (Fig. 3c). These results may
 172 be summarized as follows: (1) all ten cases can reproduce the observed spatial structure
 173 indicating that the HTHH forcing is very likely the cause of the observed anomaly; and
 174 (2) a substantial fraction (40%) of the volcanic eruption simulations has a weak signal,
 175 indicating that there is a substantial stochastic component, such that the observed re-
 176 sponse is likely but not entirely deterministic.

177 We attempted to find a mechanistic explanation for the stratospheric temperature
 178 anomalies that develop in the months following the eruption but were unable to do so.
 179 At the same time when strong stratospheric temperature anomalies occur, there is a stronger

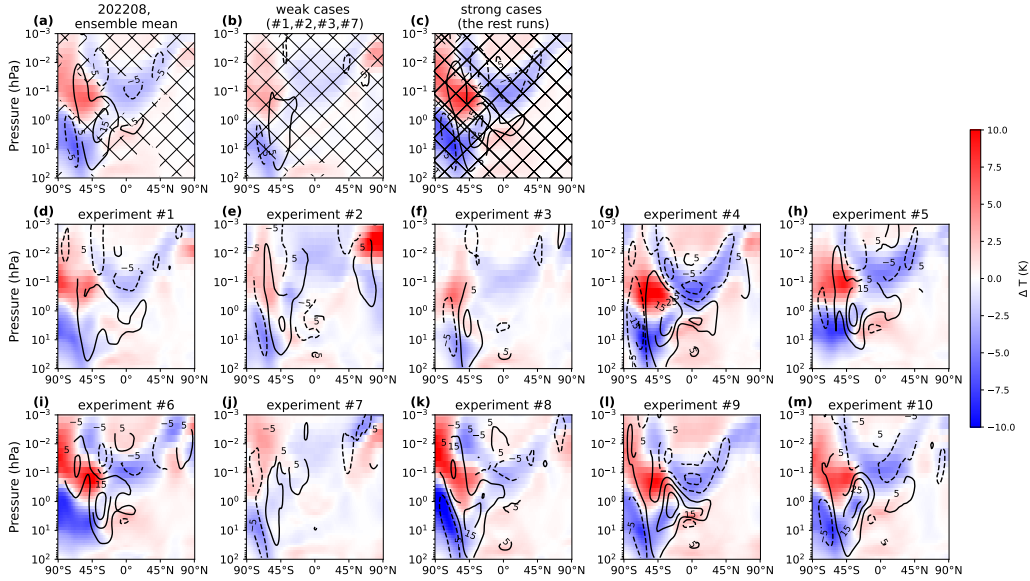


Figure 3. August 2022 zonal mean temperature difference (shading) between the volcano run and the ensemble mean control run in WACCM averaged over (a) all 10 volcanic ensemble members, (b) volcanic weak cases (case numbers 4,5,7), and (c) volcanic strong cases (the remainder of the cases in the volcanic ensemble). The areas with differences that have a p-value > 0.05 in a t-test are indicated by hatching. (d-m) The zonal mean temperature difference and zonal wind difference (contour) between each volcano run and the ensemble mean control run in WACCM. The date when nudging ends in WACCM is 27 January 2022 to 5 February 2022 in cases 1-10, respectively.

180 polar jet, a weakening in the planetary wave amplitude (mostly zonal wave 1), and thus
 181 weakening planetary wave drag (EP flux divergence) over SH mid-latitudes. This is a
 182 pattern of natural internal variability has been described in previous studies (e.g. Holton
 183 & Mass, 1976; Randel & Newman, 1998). We investigated the role of possible precu-
 184 sors to this pattern, in the months immediately following the eruption and before June,
 185 but we did not find statistically significant differences among the August strong and weak
 186 cases. The precursors we examined include radiative forcing from water vapor or sulfate
 187 aerosols, gravity wave drag, planetary wave propagation conditions, EP flux and EP flux
 188 divergence, meridional and zonal wind, and tropical and subtropical temperatures. We
 189 also examined the behavior of the quasi-biennial oscillation and found no statistically
 190 significant differences in amplitude or phase. Furthermore, we found that the strong and
 191 weak cases in July but are not always the same as the strong and weak cases in August.
 192 Finally, we have identified similar patterns of stratospheric temperature anomalies, al-
 193 though with somewhat weaker amplitude (within ± 7 K), to those observed in August
 194 in three control cases where no volcanic forcing is present. We conclude from these WACCM6
 195 simulations that the strong July/August response in stratospheric temperature is partly
 196 stochastic, although the volcanic forcing (H_2O+SO_2) significantly increases the proba-
 197 bility that the system will develop the observed SH system.

198 In contrast to the stratosphere, it is relatively simple to understand mechanistically
 199 the development of mesospheric temperature anomalies once the stratospheric changes
 200 are in place. In what follows, we focus on August 2022, the month with the strongest
 201 temperature response in both the stratosphere and mesosphere. We partition the meso-

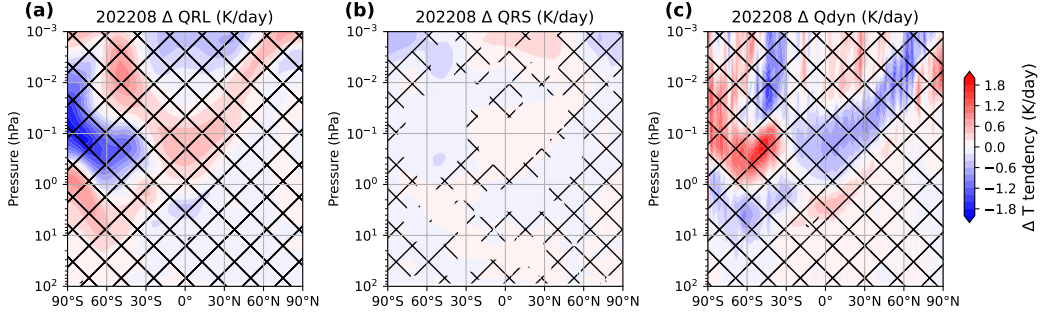


Figure 4. Latitude-pressure distribution of terms in the zonal-mean temperature budget in WACCM in August of 2022. The plots show the 10-member ensemble mean difference between the volcano case and the control case for (a) longwave heating rate, (b) shortwave heating rate, and (c) heating rate related to dynamics. The areas with differences that have a p-value > 0.05 in a t-test are indicated by hatching.

202

spheric temperature budget into contributions from radiation and dynamics, using the transformed Eulerian mean (TEM) thermodynamic equation (Andrews et al., 1987):

203

$$\frac{\partial \bar{T}}{\partial t} = -w^* S - v^* \frac{\partial \bar{T}}{a \partial \phi} + QRL + QRS \quad (1)$$

204

Where $\frac{\partial \bar{T}}{\partial t}$ is the rate of temperature change, v^* and w^* are the TEM meridional and vertical velocities, S is the static stability, QRL and QRS are the longwave and shortwave heating rates, a is the Earth’s radius and ϕ is latitude. On a monthly mean basis, $\frac{\partial \bar{T}}{\partial t}$ is expected to be small, and QRL reflects the changes in temperature (Wehrbein & Leovy, 1982), so we have:

205

206

207

208

$$QRL = -(Q_{dyn} + QRS) \quad (2)$$

209

where:

$$Q_{dyn} = -w^* S - v^* \frac{\partial \bar{T}}{a \partial \phi} \quad (3)$$

210

Our model results suggest that changes in dynamics (which produce adiabatic cooling or warming) are the primary contributor to mesospheric temperature changes (Fig. 4). Although there are some regions where the difference in the mesospheric shortwave heating rate between the volcano case and control case is significant, changes in shortwave heating rate in response to the volcanic eruption are negligible with respect to other terms in Eq. (1).

211

212

213

214

215

216

The mean meridional circulation determines Q_{dyn} in the mesosphere. Following the HTHH eruption, there was a $\sim 20\%$ strengthening of the mesospheric mean meridional circulation, which peaked in August of 2022, as shown by the red arrows in Fig. 5c. The polar winter SH shows strongly enhanced descending motion of $\sim 0.003 \text{ ms}^{-1}$ between 0.1 hPa and 0.01 hPa, corresponding to the warm temperature anomaly seen in Fig. 3. In the summer Northern Hemisphere (NH), there is a weak acceleration in the ascending motion of $\sim 0.002 \text{ ms}^{-1}$ above 0.1 hPa. In the tropical regions of both hemispheres, the horizontal mean flow accelerates by $\sim 1 \text{ ms}^{-1}$ at around 0.1 hPa. The acceleration

217

218

219

220

221

222

223

224 of the mesospheric circulation in the tropics and the summer hemisphere coincides with
 225 the V-shaped region of cooling there (Fig. 2).

226 We attribute the strengthening of the mean meridional circulation in the mesosphere
 227 to the strengthening of the stratospheric westerlies, and their resultant effects on filter-
 228 ing vertically propagating gravity waves. As mentioned by Coy et al. (2022) and Wang
 229 et al. (2022), the stratospheric westerlies undergo strengthening and an equatorward shift
 230 in SH winter 2022, and this is also what we find in the ensemble of the volcanic simu-
 231 lations (see Fig. 5f). These stratospheric zonal wind changes are in balance with reduced
 232 planetary wave EP flux divergences (Fig. 5l). Changes in the stratospheric westerlies are
 233 consistent with the geostrophic wind that is derived from the meridional temperature
 234 gradient (Harvey et al., 2022; Holton, 2004, p.200) The strengthening of the stratospheric
 235 westerly jet between about 20°S and 60°S filters eastward propagating gravity waves in
 236 the (parameterized) gravity wave spectrum. This, in turn, enhances the net westward
 237 momentum flux reaching the mesosphere. As a result, westward gravity wave drag in-
 238 creases above 0.1 hPa (i.e., the drag becomes more negative, Fig. 5i), which accelerates
 239 the mesospheric meridional circulation in SH mid-latitudes above the region where the
 240 stratospheric westerlies have intensified (Fig. 5c). Although the forcing due to planetary
 241 waves in the mid-latitudes of the SH mesosphere weakens, as shown by the reduced (less
 242 negative) EP-flux divergence in Fig. 5l, it offsets only partially the increase in westward
 243 momentum deposited by the stronger gravity wave breaking. The combination of grav-
 244 ity wave drag and EP flux divergence produces a negative forcing anomaly (Fig. 5o) that
 245 is consistent with the acceleration of the meridional circulation seen in Fig. 5c.

246 The effect of the changes in the mean meridional circulation is reflected in the pat-
 247 tern of Q_{dyn} in the SH mid-latitudes shown in Fig. 4c. The acceleration of the merid-
 248 ional circulation in the SH mid-latitudes extends across the tropics and into the NH, show-
 249 ing a pattern similar to that found during interhemispheric coupling events, along with
 250 concomitant changes in temperature and zonal wind (cf. Smith et al., 2020, their Fig.4).
 251 Changes in gravity wave drag are also reflected in changes in the mesospheric zonal wind
 252 (Fig. 5f) since wave drag tends to accelerate or decelerate the mean flow toward the wave
 253 phase speed. An increase in the westward wave drag between 0.1 – 0.2 hPa in the sub-
 254 tropics leads to a weakening of the eastward zonal wind of $\sim 10 \text{ m s}^{-1}$ there.

255 4 Discussion

256 In 2022, SABER stratospheric and mesospheric temperatures exhibited statistically
 257 significant changes, with record highs and lows observed in the stratosphere and meso-
 258 sphere in August. Our study, based on fully-coupled simulations carried out with WACCM,
 259 shows good agreement with the observed temperature anomalies in the mesosphere. The
 260 model suggests the temperature anomalies in the mesosphere are a result of a global strength-
 261 ening of the mesospheric meridional circulation of $\sim 20\%$. Through our analysis of the
 262 model, we have found that the changes in mesospheric dynamics observed in response
 263 to the HTHH volcanic eruption can be linked to dynamical changes occurring in the strato-
 264 sphere, such as the strengthening of the westerlies, altered gravity wave propagation, the
 265 weakening of planetary wave dissipation, and the weakening of the Brewer-Dobson cir-
 266 culation.

267 The causal relationship between strengthening of the stratospheric westerlies and
 268 the mesospheric temperature anomalies is robust. In all the strong cases of the WACCM
 269 volcanic ensemble where the temperature field tripolar structure has an amplitude com-
 270 parable to the observations, there is a strong strengthening and equatorward shift of the
 271 stratospheric westerlies, and in all the weak cases the stratospheric westerlies strengthen
 272 only weakly (Fig. 3). The timing of the strongest response in the mesosphere in 2022
 273 also indicates that changes in the stratosphere are the cause of the changes in the meso-
 274 sphere. The mesospheric circulation is strongest near the solstice, while in June the tem-

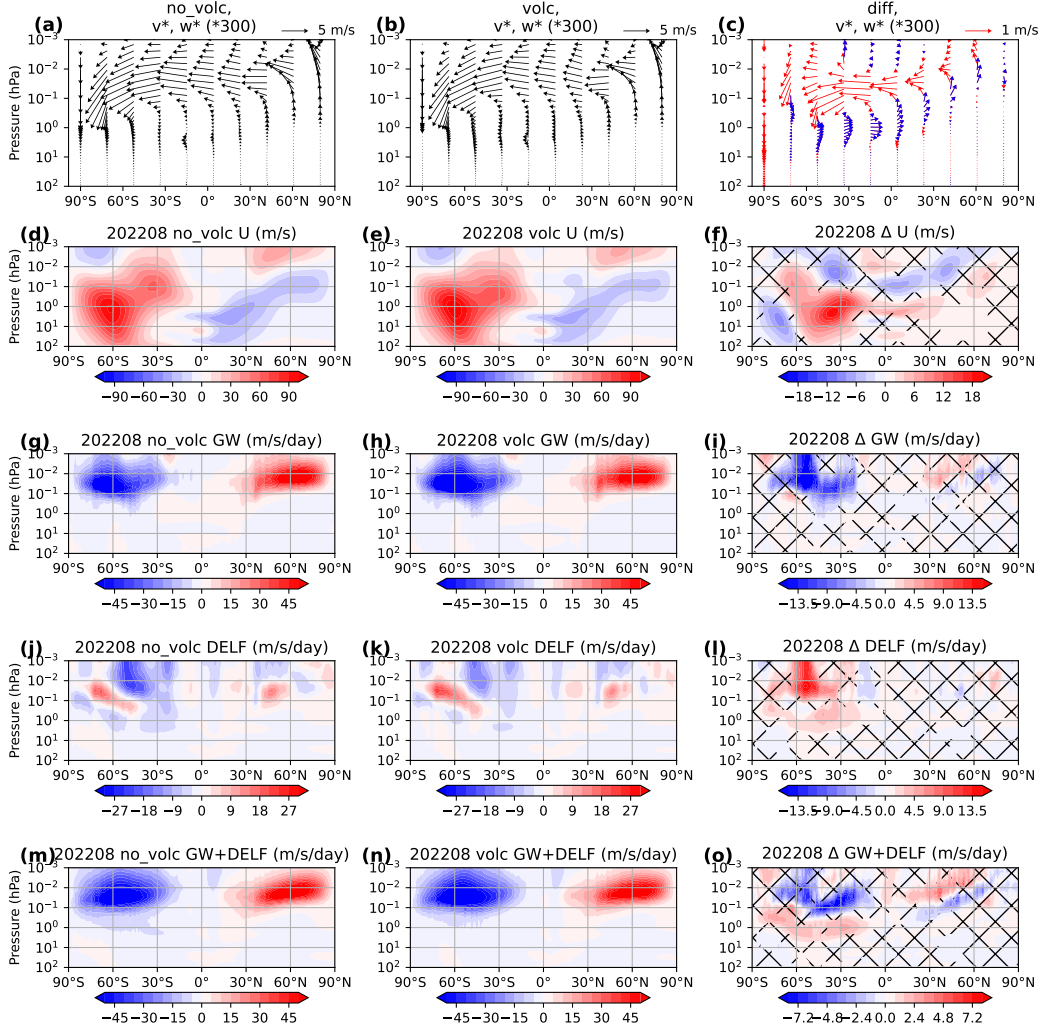


Figure 5. Zonal mean distribution of the WACCM 10-member ensemble mean for various quantities in August of 2022. (a-c) TEM circulation vectors (v^* and $300 \times w^*$ for scaling), (d-f) zonal wind, (g-i) gravity wave drag, (j-l) EP-flux divergence, and (m-o) gravity wave drag plus the EP-flux divergence. The left column shows the control case, the middle column shows the volcano case, and the right column shows the difference between the volcano case minus the control case, where the areas with differences that have a p-value > 0.05 in a t-test are indicated by hatching. In (c), red arrows indicate a strengthening of the mean meridional velocity vector and blue arrows indicate a weakening thereof compared to the control case.

275 perature difference is insignificant. The strongest mesospheric temperature response oc-
 276 curs in August when the strengthening of the westerlies is largest in the stratosphere.
 277 It is also worth mentioning that in early 2023 neither the model nor the observations show
 278 a strong disturbance in stratospheric westerlies, or in the mesospheric temperature and
 279 circulation.

280 Since what happens in the mesosphere is a response to changes in the stratosphere,
 281 there are questions regarding changes in stratospheric dynamics itself. The facts that
 282 (1) not every member of the ensemble reproduces well the observed changes, and (2) the
 283 ensemble members that reproduce most closely the observed changes are not the same
 284 in July and August suggest that there is a stochastic component in the model results.
 285 We also attempted to find precursors for the changes in the stratosphere (radiative forc-
 286 ing, EP fluxes, meridional and zonal winds, tropical and subtropical temperatures), but
 287 were unable to find any statistically significant precursors for the large, significant changes
 288 that take place in July and August in the strong group of volcano ensemble members.

289 There remain many unsolved questions related to the abrupt changes seen in the
 290 stratosphere after the HTHH eruption. For example, what is the initial driver for the
 291 strong reduction of the SH planetary wave drag in the stratosphere in July and August?
 292 Is it the injected water vapor or the aerosols, or something else? Coy et al. (2022) sug-
 293 gested that the changes before June are due to the injected water vapor. As shown in
 294 our Fig. 2, there is a significant cooling in the stratosphere collocated with the injected
 295 water vapor anomaly before June. However, starting in June, a large, negative strato-
 296 spheric temperature anomaly develops in the midlatitudes of the SH over a much broader
 297 altitude range. Since this anomaly is no longer collocated with the water vapor anomaly,
 298 it must be due to dynamical changes. However, as noted above, we were unable to iden-
 299 tify any precursors to these changes. In addition, it is unclear why the stratospheric wind
 300 and circulation anomalies intensify suddenly in July and August. While the investiga-
 301 tion of these stratospheric questions is outside the scope of our paper, addressing them
 302 would enhance our understanding of middle atmospheric dynamics and provide further
 303 insights into the HTHH volcanic eruption.

304 5 Open Research

305 - [Dataset] SABER v2.07 and v2.08 temperature data are available from [https://](https://saber.gats-inc.com/data_services.php)
 306 saber.gats-inc.com/data_services.php, See Mlynczak et al. (2023)

307 - [Software] CESM2-WACCM6 codes are available from [//www.cesm.ucar.edu/](http://www.cesm.ucar.edu/models/cesm2)
 308 [models/cesm2](http://www.cesm.ucar.edu/models/cesm2). See Gettelman et al. (2019).

309 Acknowledgments

310 WY, RG, JY, and MM are supported by the TIMED/SABER mission from the NASA
 311 Heliophysics Division. WY and JY are also supported by NASA’s Heliophysics Division
 312 AIM mission and NSF AGS1901126. RG is supported in part by NASA grant 80NSSC19K1214.
 313 ZQ is supported by NSF AGS-1828589. The National Center for Atmospheric Research
 314 is sponsored by the National Science Foundation. Work conducted at CIRES/NOAA is
 315 supported by the NOAA’s Earth Radiation Budget (ERB) Initiative (CPO #03-01-07-
 316 001), and in part by NOAA cooperative agreements NA17OAR4320101 and NA22OAR4320151.
 317 We thank Dr. James Russell III for his support and encouragement as an advisor at HU,
 318 and thank National Center for Atmospheric Research (NCAR) Atmospheric Chemistry
 319 Observations & Modeling (ACOM) for hosting WY’s visit during this work. NCAR is
 320 sponsored by the U.S. National Science Foundation (NSF). WACCM is a component of
 321 the Community Earth System Model (CESM), which is supported by NSF and the Of-
 322 fice of Science of the U.S. Department of Energy. Computing resources for the results
 323 presented here were provided by NCAR’s Climate Simulation Laboratory, sponsored by

324 NSF and other agencies, and enabled by the computational and storage resources of NCAR's
 325 Computational and Information Systems Laboratory (CISL).

326 References

- 327 Andrews, D. G., Holton, J. R., & Leovy, C. B. (1987). *Middle atmosphere dynam-*
 328 *ics. no. 40. academic press, 1987.* Academic Press.
- 329 Carn, S. A., Krotkov, N. A., Fisher, B. L., & Li, C. (2022). Out of the blue: Vol-
 330 canic so₂ emissions during the 2021–2022 eruptions of hunga tonga—hunga
 331 ha'apai (tonga). *Frontiers in Earth Science, 10*. Retrieved from [https://](https://www.frontiersin.org/articles/10.3389/feart.2022.976962)
 332 www.frontiersin.org/articles/10.3389/feart.2022.976962 doi:
 333 10.3389/feart.2022.976962
- 334 Coy, L., Newman, P. A., Wargan, K., Partyka, G., Strahan, S. E., & Pawson, S.
 335 (2022). Stratospheric circulation changes associated with the hunga tonga-
 336 hunga ha'apai eruption. *Geophysical Research Letters, 49*(22), e2022GL100982.
 337 Retrieved from [https://onlinelibrary.wiley.com/doi/abs/10.1029/](https://onlinelibrary.wiley.com/doi/abs/10.1029/2022GL100982)
 338 [2022GL100982](https://onlinelibrary.wiley.com/doi/abs/10.1029/2022GL100982) doi: 10.1029/2022GL100982
- 339 Dawkins, E. C., Feofilov, A., Rezac, L., Kutepov, A. A., Janches, D., Höffner, J., ...
 340 Russell, J. (2018). Validation of saber v2.0 operational temperature data with
 341 ground-based lidars in the mesosphere-lower thermosphere region (75–105 km).
 342 *Journal of Geophysical Research: Atmospheres, 123*(17), 9916–9934. doi:
 343 10.1029/2018JD028742
- 344 Dunkerton, T. (1978, 12 1). On the mean meridional mass motions of the strato-
 345 sphere and mesosphere. *Journal of the Atmospheric Sciences, 35*(12), 2325–
 346 2333. Retrieved from [https://journals.ametsoc.org/view/journals/](https://journals.ametsoc.org/view/journals/atsc/35/12/1520-0469_1978_035_2325_otmmmm_2_0_co_2.xml)
 347 [atsc/35/12/1520-0469_1978_035_2325_otmmmm_2_0_co_2.xml](https://journals.ametsoc.org/view/journals/atsc/35/12/1520-0469_1978_035_2325_otmmmm_2_0_co_2.xml) doi: 10.1175/
 348 1520-0469(1978)035{\textless}2325:OTMMMM{\textgreater}2.0.CO;2
- 349 Garcia, R. R., & Solomon, S. (1985). The effect of breaking gravity waves
 350 on the dynamics and chemical composition of the mesosphere and lower
 351 thermosphere. *Journal of Geophysical Research, 90*(D2), 3850. Re-
 352 trieved from <http://doi.wiley.com/10.1029/JD090iD02p03850> doi:
 353 10.1029/JD090iD02p03850
- 354 García-Comas, M., López-Puertas, M., Marshall, B. T., Wintersteiner, P. P., Funke,
 355 B., Bermejo-Pantaleón, D., ... Russell III, J. M. (2008). Errors in sounding
 356 of the atmosphere using broadband emission radiometry (saber) kinetic tem-
 357 perature caused by non-local-thermodynamic-equilibrium model parameters.
 358 *Journal of Geophysical Research: Atmospheres, 113*(D24). Retrieved from
 359 <https://onlinelibrary.wiley.com/doi/abs/10.1029/2008JD010105> doi:
 360 10.1029/2008JD010105
- 361 Gettelman, A., Mills, M. J., Kinnison, D. E., Garcia, R. R., Smith, A. K., Marsh,
 362 D. R., ... Randel, W. J. (2019). The whole atmosphere community climate
 363 model version 6 (waccm6). *Journal of Geophysical Research: Atmospheres,*
 364 *124*(23), 12380–12403. doi: 10.1029/2019JD030943
- 365 Harvey, V. L., Pedatella, N., Becker, E., & Randall, C. (2022, 8 16). Evaluation
 366 of polar winter mesopause wind in waccmx+dart. *Journal of Geophysical Re-*
 367 *search: Atmospheres, 127*(15). Retrieved from [https://onlinelibrary.wiley](https://onlinelibrary.wiley.com/doi/10.1029/2022JD037063)
 368 [.com/doi/10.1029/2022JD037063](https://onlinelibrary.wiley.com/doi/10.1029/2022JD037063) doi: 10.1029/2022JD037063
- 369 Holton, J. R. (1983, 10 1). The influence of gravity wave breaking on the general
 370 circulation of the middle atmosphere. *Journal of the Atmospheric Sciences,*
 371 *40*(10), 2497–2507. Retrieved from [https://journals.ametsoc.org/view/](https://journals.ametsoc.org/view/journals/atsc/40/10/1520-0469_1983_040_2497_tiogwb_2_0_co_2.xml)
 372 [journals/atsc/40/10/1520-0469_1983_040_2497_tiogwb_2_0_co_2.xml](https://journals.ametsoc.org/view/journals/atsc/40/10/1520-0469_1983_040_2497_tiogwb_2_0_co_2.xml) doi:
 373 10.1175/1520-0469(1983)040<2497:TIOGWB>2.0.CO;2
- 374 Holton, J. R. (2004). *An introduction to dynamic meteorology* (4th ed.; R. Dmowska
 375 & J. R. Holton, Eds.). Burlington, MA: Elsevier Academic Press,. Retrieved
 376 from <http://books.google.com/books?id=fhW5oDv3EPsC>

- 377 Holton, J. R., & Mass, C. (1976, 11 1). Stratospheric vacillation cycles. *Journal*
378 *of the Atmospheric Sciences*, *33*(11), 2218–2225. Retrieved from [https://](https://journals.ametsoc.org/view/journals/atasc/33/11/1520-0469_1976_033_2218_svc_2.0_co_2.xml)
379 [journals.ametsoc.org/view/journals/atasc/33/11/1520-0469_1976_033](https://journals.ametsoc.org/view/journals/atasc/33/11/1520-0469_1976_033_2218_svc_2.0_co_2.xml)
380 [_2218_svc_2.0_co_2.xml](https://journals.ametsoc.org/view/journals/atasc/33/11/1520-0469_1976_033_2218_svc_2.0_co_2.xml) doi: 10.1175/1520-0469(1976)033{\textless}2218:
381 SVC{\textgreater}2.0.CO;2
- 382 Khaykin, S., Podglajen, A., Ploeger, F., Grooß, J.-U., Tence, F., Bekki, S., ...
383 Ravetta, F. (2022, 12 14). Global perturbation of stratospheric water and
384 aerosol burden by hunga eruption. *Communications Earth & Environ-*
385 *ment*, *3*(1), 1–15. Retrieved from [https://www.nature.com/articles/](https://www.nature.com/articles/s43247-022-00652-x)
386 [s43247-022-00652-x](https://www.nature.com/articles/s43247-022-00652-x) doi: 10.1038/s43247-022-00652-x
- 387 Lindzen, R. S. (1981). Turbulence and stress owing to gravity wave and
388 tidal breakdown. *Journal of Geophysical Research*, *86*(C10), 9707. Re-
389 trieved from <http://doi.wiley.com/10.1029/JC086iC10p09707> doi:
390 [10.1029/JC086iC10p09707](http://doi.wiley.com/10.1029/JC086iC10p09707)
- 391 Livesey, N. J., Read, W., Lambert, A., Cofield, R., Cuddy, D., Froidevaux, L., ...
392 Co, R. E. (2020). *Earth observing system (eos) aura microwave limb sounder*
393 *(mls) description document* (Tech. Rep.).
- 394 Millán, L., Santee, M. L., Lambert, A., Livesey, N. J., Werner, F., Schwartz, M. J.,
395 ... Froidevaux, L. (2022). The hunga tonga-hunga ha’apai hydration of the
396 stratosphere. *Geophysical Research Letters*, *49*(13), e2022GL099381. Retrieved
397 from <http://onlinelibrary.wiley.com/doi/abs/10.1029/2022GL099381>
398 doi: 10.1029/2022GL099381
- 399 Mlynczak, M. G., Daniels, T., Hunt, L. A., Yue, J., Marshall, B. T., Russell, J. M.,
400 ... Yee, J. H. (2020). Radiometric stability of the saber instrument. *Earth and*
401 *Space Science*, *7*(2), e2019EA001011. doi: 10.1029/2019EA001011
- 402 Mlynczak, M. G., Marshall, B. T., Garcia, R. R., Hunt, L., Yue, J., Harvey, V. L.,
403 ... Russell, J. (2023, 3 16). Algorithm stability and the long-term geospace
404 data record from timed/saber. *Geophysical Research Letters*, *50*(5). Retrieved
405 from <https://onlinelibrary.wiley.com/doi/10.1029/2022GL102398> doi:
406 [10.1029/2022GL102398](https://onlinelibrary.wiley.com/doi/10.1029/2022GL102398)
- 407 Proud, S. R., Prata, A. T., & Schmauß, S. (2022, 11 4). The january 2022 erup-
408 tion of hunga tonga-hunga ha’apai volcano reached the mesosphere. *Science*,
409 *378*(6619), 554–557. Retrieved from [http://www.science.org/doi/10.1126/](http://www.science.org/doi/10.1126/science.abo4076)
410 [science.abo4076](http://www.science.org/doi/10.1126/science.abo4076) doi: 10.1126/science.abo4076
- 411 Randall, C. E., Harvey, V. L., Siskind, D. E., France, J., Bernath, P. F., Boone,
412 C. D., & Walker, K. A. (2009). Nox descent in the arctic middle atmo-
413 sphere in early 2009. *Geophysical Research Letters*, *36*(18). Retrieved from
414 <https://onlinelibrary.wiley.com/doi/abs/10.1029/2009GL039706> doi:
415 [10.1029/2009GL039706](https://onlinelibrary.wiley.com/doi/abs/10.1029/2009GL039706)
- 416 Randel, W. J., Johnston, B. R., Braun, J. J., Sokolovskiy, S., Vömel, H., Podglajen,
417 A., & Legras, B. (2023, 1). Stratospheric water vapor from the hunga
418 tonga–hunga ha’apai volcanic eruption deduced from cosmic-2 radio occul-
419 tation. *Remote Sensing*, *15*(8), 2167. Retrieved from [https://www.mdpi.com/](https://www.mdpi.com/2072-4292/15/8/2167)
420 [2072-4292/15/8/2167](https://www.mdpi.com/2072-4292/15/8/2167) doi: 10.3390/rs15082167
- 421 Randel, W. J., & Newman, P. A. (1998). The stratosphere in the southern hemi-
422 sphere. In D. J. Karoly & D. G. Vincent (Eds.), *Meteorology of the southern*
423 *hemisphere* (pp. 243–282). Boston, MA: American Meteorological Society. Re-
424 trieved from https://doi.org/10.1007/978-1-935704-10-2_9
- 425 Remsberg, E., Marshall, B. T., Garcia-Comas, M., Krueger, D., Lingenfelter, G. S.,
426 Martin-Torres, J., ... Thompson, R. E. (2008). Assessment of the quality of
427 the version 1.07 temperature-versus-pressure profiles of the middle atmosphere
428 from timed/saber. *Journal of Geophysical Research: Atmospheres*, *113*(D17),
429 17101. doi: 10.1029/2008JD010013
- 430 Rienecker, M., Suarez, M., Todling, R., Bacmeister, J., Takacs, L., Liu, H.-C., ...
431 Nielsen, J. (2018). *The geos-5 data assimilation system— documentation of*

- versions 5.0.1, 5.1.0, and 5.2.0 (Tech. Rep.).
- Russell, J. M., Mlynczak, M. G., Gordley, L. L., Tansock, J. J., Jr., & Esplin, R. W. (1999, 10 20). Overview of the saber experiment and preliminary calibration results. In (Vol. 3756, p. 277). International Society for Optics and Photonics. Retrieved from <https://www.spiedigitallibrary.org/conference-proceedings-of-spie/3756/0000/Overview-of-the-SABER-experiment-and-preliminary-calibration-results/10.1117/12.366382.full> doi: 10.1117/12.366382
- Schoeberl, M. R., Wang, Y., Ueyama, R., Taha, G., Jensen, E., & Yu, W. (2022). Analysis and impact of the hunga tonga-hunga ha'apai stratospheric water vapor plume. *Geophysical Research Letters*, *49*(20), e2022GL100248. Retrieved from <https://onlinelibrary.wiley.com/doi/abs/10.1029/2022GL100248> doi: 10.1029/2022GL100248
- Sellitto, P., Podglajen, A., Belhadji, R., Boichu, M., Carboni, E., Cuesta, J., ... Legras, B. (2022, 11 19). The unexpected radiative impact of the hunga tonga eruption of 15th january 2022. *Communications Earth & Environment*, *3*(1), 1–10. Retrieved from <http://www.nature.com/articles/s43247-022-00618-z> doi: 10.1038/s43247-022-00618-z
- Smith, A. K., Garcia, R. R., Marsh, D. R., & Richter, J. H. (2011, 10 20). Waccm simulations of the mean circulation and trace species transport in the winter mesosphere. *Journal of Geophysical Research*, *116*(D20), D20115. Retrieved from <http://doi.wiley.com/10.1029/2011JD016083> doi: 10.1029/2011JD016083
- Smith, A. K., Marsh, D. R., Mlynczak, M. G., & Mast, J. C. (2010). Temporal variations of atomic oxygen in the upper mesosphere from saber. *Journal of Geophysical Research: Atmospheres*, *115*(D18). Retrieved from <https://onlinelibrary.wiley.com/doi/abs/10.1029/2009JD013434> doi: 10.1029/2009JD013434
- Smith, A. K., Pedatella, N. M., & Mullen, Z. K. (2020, 3 1). Interhemispheric coupling mechanisms in the middle atmosphere of waccm6. *Journal of the Atmospheric Sciences*, *77*(3), 1101–1118. Retrieved from <https://journals.ametsoc.org/view/journals/atsc/77/3/jas-d-19-0253.1.xml> doi: 10.1175/JAS-D-19-0253.1
- Taha, G., Loughman, R., Colarco, P. R., Zhu, T., Thomason, L. W., & Jaross, G. (2022). Tracking the 2022 hunga tonga-hunga ha'apai aerosol cloud in the upper and middle stratosphere using space-based observations. *Geophysical Research Letters*, *49*(19), e2022GL100091. Retrieved from <http://onlinelibrary.wiley.com/doi/abs/10.1029/2022GL100091> doi: 10.1029/2022GL100091
- Vincent, R. A. (2015, 3). The dynamics of the mesosphere and lower thermosphere: a brief review. *Progress in Earth and Planetary Science*, *2*(1), 4. Retrieved from <http://www.progearthplanetosci.com/content/2/1/4> doi: 10.1186/s40645-015-0035-8
- Vömel, H., Evan, S., & Tully, M. (2022, 9 23). Water vapor injection into the stratosphere by hunga tonga-hunga ha'apai. *Science*, *377*(6613), 1444–1447. Retrieved from <https://www.science.org/doi/full/10.1126/science.abq2299> doi: 10.1126/science.abq2299
- Wang, X., Randel, W., Zhu, Y., Tilmes, S., Starr, J., Yu, W., ... Li, J. (2022, 11 26). *Stratospheric climate anomalies and ozone loss caused by the hunga tonga volcanic eruption* (Tech. Rep.). Retrieved from <https://essopenarchive.org/doi/full/10.1002/essoar.10512922.1>
- Waters, J. W., Froidevaux, L., Harwood, R. S., Jarnot, R. F., Pickett, H. M., Read, W. G., ... Walch, M. J. (2006, 5). The earth observing system microwave limb sounder (eos mls) on the aura satellite. *IEEE Transactions on Geoscience and Remote Sensing*, *44*(5), 1075–1092. doi: 10.1109/TGRS.2006.873771

- 487 Wehrbein, W. M., & Leovy, C. B. (1982, 7 1). An accurate radiative heat-
488 ing and cooling algorithm for use in a dynamical model of the middle at-
489 mosphere. *Journal of the Atmospheric Sciences*, 39(7), 1532–1544. Re-
490 trieved from [https://journals.ametsoc.org/view/journals/atsc/](https://journals.ametsoc.org/view/journals/atsc/39/7/1520-0469_1982_039_1532_aarhac_2_0_co_2.xml)
491 [39/7/1520-0469_1982_039_1532_aarhac_2_0_co_2.xml](https://journals.ametsoc.org/view/journals/atsc/39/7/1520-0469_1982_039_1532_aarhac_2_0_co_2.xml) doi: 10.1175/
492 1520-0469(1982)039<>1532:AARHAC<>2.0.CO;2
- 493 Zhu, Y., Bardeen, C. G., Tilmes, S., Mills, M. J., Wang, X., Harvey, V. L., ... Toon,
494 O. B. (2022, 10 22). Perturbations in stratospheric aerosol evolution due to the
495 water-rich plume of the 2022 hunga-tonga eruption. *Communications Earth &*
496 *Environment*, 3(1), 1–7. Retrieved from [https://www.nature.com/articles/](https://www.nature.com/articles/s43247-022-00580-w)
497 [s43247-022-00580-w](https://www.nature.com/articles/s43247-022-00580-w) doi: 10.1038/s43247-022-00580-w